LBL-23168
UC-34

Lawrence Berkeley Laboratory
UNIVERSITY OF CALIFORNIA

Accelerator & Fusion Research Division

RECEIVED
JUN 1987
DOCUMENTS SECTION

HEAVY ION FUSION ACCELERATOR RESEARCH (HIFAR)
HALF-YEAR REPORT: October 1, 1986–March 31, 1987

Heavy Ion Fusion Staff

April 1987

TWO-WEEK LOAN COPY
This is a Library Circulating Copy which may be borrowed for two weeks.

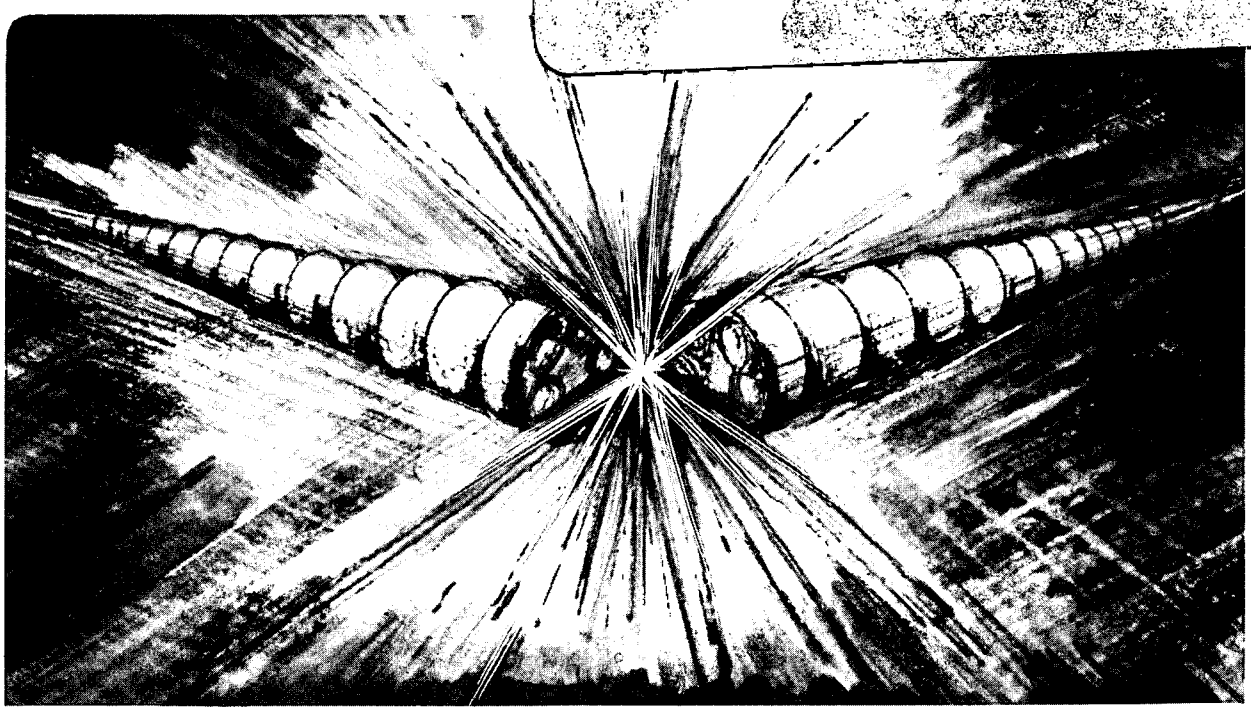

LBL-23168

Prepared for the U.S. Department of Energy under Contract DE-AC03-76SF00098

DISCLAIMER

This document was prepared as an account of work sponsored by the United States Government. While this document is believed to contain correct information, neither the United States Government nor any agency thereof, nor the Regents of the University of California, nor any of their employees, makes any warranty, express or implied, or assumes any legal responsibility for the accuracy, completeness, or usefulness of any information, apparatus, product, or process disclosed, or represents that its use would not infringe privately owned rights. Reference herein to any specific commercial product, process, or service by its trade name, trademark, manufacturer, or otherwise, does not necessarily constitute or imply its endorsement, recommendation, or favoring by the United States Government or any agency thereof, or the Regents of the University of California. The views and opinions of authors expressed herein do not necessarily state or reflect those of the United States Government or any agency thereof or the Regents of the University of California.

LBL-23168
HIFAN-362

HEAVY ION FUSION ACCELERATOR RESEARCH (HIFAR) HALF-YEAR REPORT*

October 1, 1986 - March 31, 1987

Heavy Ion Fusion Staff

Accelerator and Fusion Research

Lawrence Berkeley Laboratory
University of California
Berkeley, CA 94720

April 1987

Attention: This document is provided for DOE "Official Use". Distribution to other interested parties is made with the understanding that no information or experimental results given herein will be quoted without first obtaining the authors' permission, or until such information or results have appeared in the open literature.

*This work was supported by the Office of Energy Research, Office of Basic Energy Sciences, U.S. Department of Energy under Contract No. DE-AC03-76SF00098.

FOREWORD

The basic objective of the Heavy Ion Fusion Accelerator Research (HIFAR) program is to assess the suitability of heavy ion beam accelerators as igniters for Inertial Confinement Fusion (ICF). A specific accelerator technology, the induction linac, has been studied at the Lawrence Berkeley Laboratory and has reached the point at which its viability for ICF applications can be assessed over the next few years.

The HIFAR program addresses the generation of high-power, high-brightness beams of heavy ions, the understanding of the scaling laws in this novel physics regime, and the validation of new accelerator strategies, to cut costs. Key elements to be addressed include: 1) Beam quality limits set by transverse and longitudinal beam physics; 2) Development of induction accelerating modules, and multiple beam hardware, at affordable costs; 3) Acceleration of multiple beams with current amplification -- both new features in a linac -- without significant dilution of the optical quality of the beams; 4) Final bunching, transport, and accurate focussing on a small target.

TABLE OF CONTENTS

	Page
Highlights	1
The LBL Multiple Beam Experiments	5
Pulsers for the Induction Linac Experiment, MBE-4	10
HIF Insulator Failure	13
Experimental Measurement of Emittance Growth in Mismatched Space-Charge-Dominated Beams	14
The Effect of Nonlinear Forces on Coherently Oscillating Space-Charge-Dominated Beams	17
Space Charge Effects in a Bending Magnet System	22
Transverse Combining of Nonrelativistic Beams in a Multiple Beam Induction Linac	25
Comparison of Electric and Magnetic Quadrupole Focusing for the Low Energy End of an Induction-Linac-ICF Driver	28
Publications and Internal Notes	31
HIF Staff Roster	37
Distribution List	38

HIGHLIGHTS

T.J. Fessenden

For this report we have collected the papers presented by the HIFAR group at the IEEE Particle Accelerator Conference held in Washington D.C. on March 16-19, 1987, which essentially coincides with the end of the reporting period. In addition we report on research to determine the cause of the failures of Re-X insulator that are used as the high-voltage feed-through for the electrostatic quadrupoles on MBE-4.

During this period, the major activity of the HIFAR group again centered around the MBE-4 experiment. We experimented until mid-February with that portion of MBE-4 that was completed by the end of FY-86. At that time we shut down to install a further complement of accelerating units. Figure 1 shows a picture of MBE-4 taken in March 1987. The apparatus is now being aligned and the pulsers are being installed. Experiments with this configuration will begin in May, 1987.

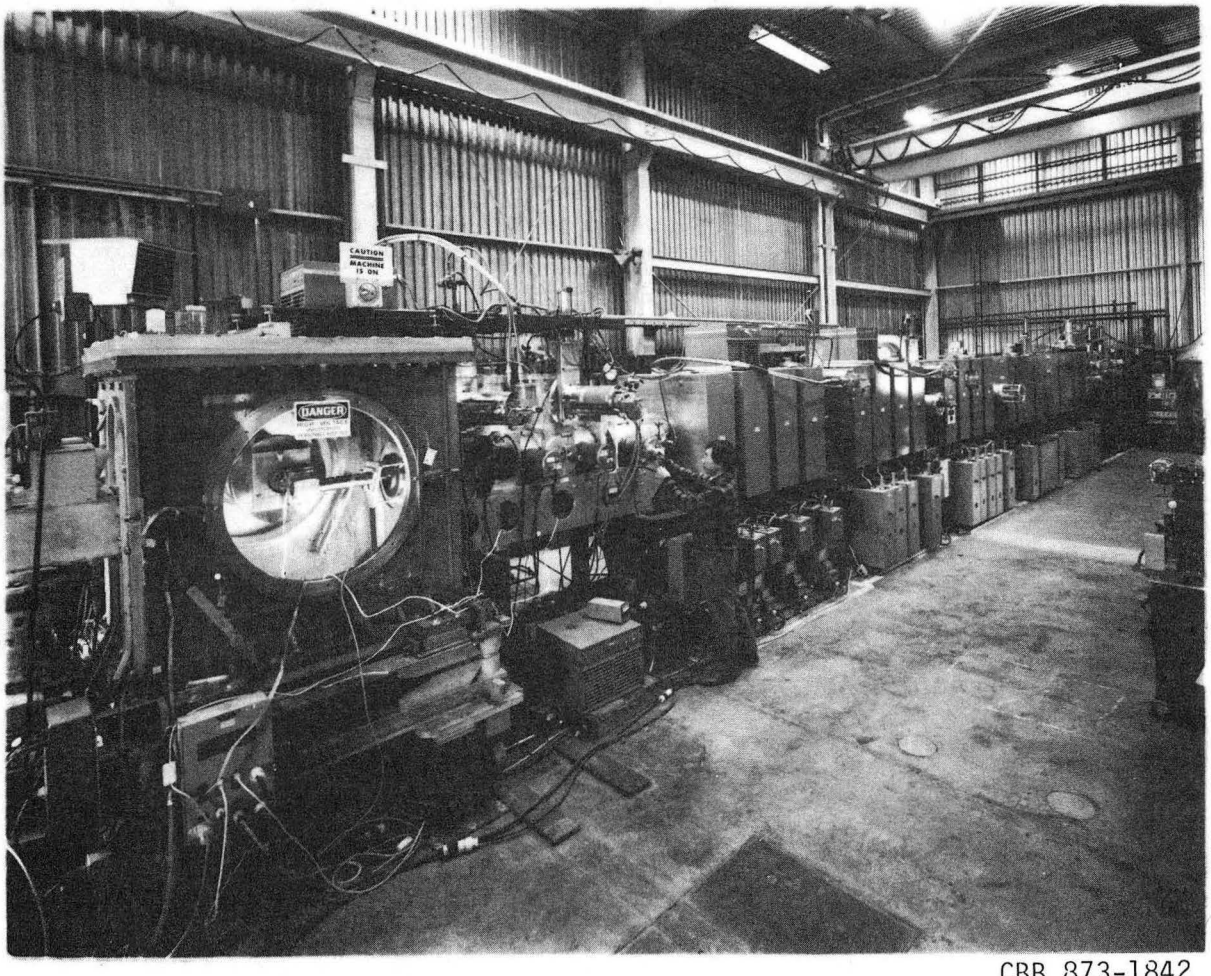

CBB 873-1842

1. Experiments with MBE-4 have thus far demonstrated amplification of the current in each of the four cesium beams from 13 to 35 mA (i.e., x 2.7) with an energy gain of 200 to 400 keV at the beam head and 200 to 550 keV at the beam tail. We are able to control the growth of current fluctuations which result from unavoidable acceleration errors by small modifications to downstream accelerating waveforms suggested by the SLID longitudinal acceleration procedure. The normalized beam emittance is remaining constant as expected except, perhaps, for some growth at the beam head. Further experiments will take place in May to August and the apparatus will be fully complete in September.

2. We have used 30 kV thyratron-switched pulsers in the first half of MBE-4. For the latter half, we will use a higher voltage pulser switched by a spark-gap. The output of a single 120 kV pulser is applied in series across two adjacent acceleration gaps. The remaining two gaps are powered by thyratron pulsers such that the net accelerating waveform for an entire four-gap section has the correct waveform to accelerate and control the length of the cesium beams. This procedure minimizes the number of pulsers required for the accelerator and, because of the higher impedance of the high-voltage pulser, provides the fast-rising accelerating waveforms needed for the last half of MBE-4.

3. As mentioned in the last report (LBL-22349), we were somewhat disturbed by failures of the metal embedments in the Re-X insulators used as high-voltage feed-throughs in MBE-4. Metallurgical tests of these have now shown the presence of small amounts of sulfur in the

metal grain boundaries of the spun metal where the failures are occurring. We hypothesize that sulfur is introduced from oil used in the spinning process. When the part is heated during welding (or possibly when the ceramic is bonded to the metal) the sulfur forms titianium-sulfide which is brittle and leads to failure as the metal is flexed. It appears that these failures can be prevented by removing the source of sulfur and/or moving the weld from the deformed area of the spun ring.

4. More details on experiments reported briefly in the last semi-annual report on the evolution of beam mis-match and emittance growth in SBTE were reported at the conference by M. Tiefenback. The experiments indicate that symmetrical beam mis-matches ($\Delta x = \Delta y$) appear to produce little or no emittance growth whereas anti-symmetrical mis-matches ($\Delta x = -\Delta y$) produce significant emittance growth as the mis-match oscillations damp along the beam line.

5. The simulation-code study of the growth of emittance for off-axis beams over hundreds of lattice periods at high tune depressions has continued. The growth is generated by effects due to image charges induced by off-axis beams, or by deviations of the quadrupole focusing fields from the ideal. The simulations show (surprisingly) that the effects of images and higher-order multipole expansions of the focusing fields tend to cancel even though these two forces seem to drive different modes. The mechanism of cancellation, however, is not yet understood.

6. Bending space-charge-dominated particle beams is an important element in many accelerator systems including those required by Heavy Ion Fusion. We have written a beam dynamics code HICURB that is being used to study beam bending when space charge effects are important. The code contains a treatment of the beam envelope and centroid in a system of bends and quadrupoles, including image forces. (This work was supported in part by the USA SDC.)

7. Our present concept of a driver for HIF employs four-to-one beam combinations at an energy like 100 MeV to change from 64 beams down to 16 beams. A computational study of emittance growth during the combination process and some initial experiments on SBTE suggest that effects due to beam space charge and geometrical phase-space dilution will increase the beam emittance by a factor 4 to 10 depending on beam intensity. A conceptual combining system minimizes the emittance growth by focusing the beams and bringing them closely together before allowing them to mix.

8. We are re-examining the case of a purely magnetically-focused HIF driver with 16 beams in which beam combining is not necessary. In principle, 16 beams at 100 MeV can be produced either by a magnetically focused accelerator without beam combining or by a 64-beam, electrostatically focused accelerator that combines 64 beams to 16 at 100 MeV. The magnetically focused accelerator is 200 meters longer and contains 50% more volt-seconds of iron, but can result in lower emittance should that be deemed desirable.

THE LBL MULTIPLE BEAM EXPERIMENTS*

Thomas J. Fessenden, Denis Keefe, Charles Kim, Hermann Meuth, and Anthony Warwick†
Lawrence Berkeley Laboratory
University of California, Berkeley, CA 94720

Summary

The multiple-beam induction linac approach to a heavy ion driver for inertial confinement fusion features continuous current amplification along the accelerator and a minimum of beam manipulations from source to pellet. Current amplification and bunch length control require careful shaping of the accelerating voltages.

MBE-4 is designed as a four-beam induction linac that models much of the accelerator physics of the electrostatically focused section of a significantly longer induction accelerator. Four space-charge-dominated Cs^+ beams, initially about one meter in length at a current of 13 mA, are focused by electrostatic quadrupoles and accelerated in parallel from 200 to nearly 600 keV. The energy will reach approximately one MeV when the accelerator is complete. Experiments have proceeded in parallel with the construction of the apparatus which began in FY 85 and is now more that half complete. The results show a current amplification, so far, by a factor of 2.8 in good agreement with the longitudinal acceleration calculations.

Introduction

The multiple beam induction accelerator experiment MBE-4 was designed to model the longitudinal physics of the electrostatically focused section of a much longer induction linac. The length of the beam bunches are short compared with the length of the accelerator and longitudinal space charge spreading must be controlled. In the completed accelerator, the current of each beam will increase by a factor of four to six and the beam energy will increase by nearly five-times. Thus the increase in beam power (VxI) will be a factor of 20 to 30. MBE-4 will demonstrate current magnification resulting largely from an increase in particle speed, but also from some shortening of the length of the beam bunch. As a percentage of beam energy, the acceleration voltages in MBE-4 are much larger than will be used in a driver. Therefore, the consequences of errors in acceleration voltages will be more apparent and more easily assessed.

Four beams are used to investigate potential effects caused by beam-beam coupling and to get practical experience in difficulties associated with accelerating and transversely controlling parallel beams. In examining the scaling with injection energy and with quadrupole size, we have been careful to preserve space-charge domination of the beams both transversely (depends on beam current density) and longitudinally (depends on line density of charge). Measured in units of initial-bunch-length, MBE-4 is comparable in length to the electrostatically focused portion of a fusion driver. In this paper we present the results of experiments with the first half of the accelerator.

An essential element in both the synthesis of the MBE-4 accelerating waveforms and the analysis of the experiments is the longitudinal acceleration procedure developed by C. Kim with help from L. Smith [1]. This method follows the longitudinal motion of the beam particles through the accelerator and includes the effects produced by beam space charge and finite gap width; it is incorporated into the computer code, SLID, which runs on a small computer. We use this code to find the accelerating waveforms at each gap in the accelerator that will produce the desired current waveforms at any position in the accelerator. For the MBE-4 design, we have chosen to specify a rectangular current pulse which remains self-similar as the current amplifies along the accelerator. Accelerating waveforms calculated by SLID are used as the initial specification for the engineering design of the accelerator pulsers [2]. Since it is not possible to synthesize exactly the ideal waveforms, we use the code to solve for slightly modified downstream accelerating waveforms that can correct for upstream errors.

Description of the MBE-4 Apparatus

Much of the mechanical design of the apparatus was presented at the IEEE Particle Accelerator Conference in Vancouver in 1985 [3]. A schematic diagram of the experiment is presented in Fig. 1. The experiment uses four beams of singly charged cesium obtained from four thermionic alumino-silicate sources. These are accelerated

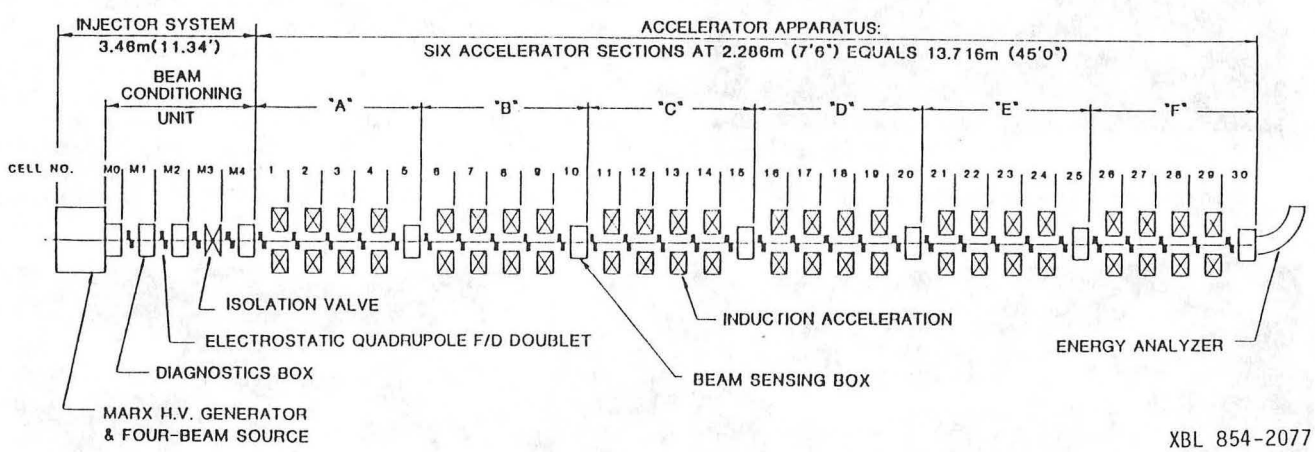

Fig. 1. Schematic Diagram of MBE-4.

*Work supported by the Office of Energy Research, Office of Basic Energy Sciences, U.S. Department of Energy under Contract DE-AC03-76SF00098.

†Now at GSI Darmstadt

to 0.2 MV in a single gap injector [4]. The initial pulse duration is 2.5 μs which will shorten to 0.6 μs at the end of the accelerator. The four beams are focused by arrays of electrostatic quadrupoles, each consisting of nine electrodes. A photograph of a quadrupole array is shown in Fig. 2. The beam-to-beam spacing is 6.67 cm (between centers) and the clear aperture diameter is 5.41 cm. The diameters of the electrodes are 4.02 cm. The electrodes occupy approximately one half the lattice period (45.7 cm). Each of the four beams is axi-symmetric at the exit of the injector, and has its envelope carefully adjusted in a electrostatic quadrupole beam matching section to the proper form for acceptance by the FODO transport system in the accelerator. The beams, each approximately one meter in length, will be accelerated to nearly 1.0 MV by 24 linear induction modules in a total length of 17.2 m. The voltage waveforms on the early accelerator gaps are nearly triangular so as to impart an axial velocity shear, or tilt, to the beam by accelerating the tail of the beam more than the head. A report [5] on the status of the development of pulsers for MBE-4 is being presented at this conference. After the tail of the beam has entered the accelerator, the head of the beam can be accelerated as well; thereafter, the waveforms on the downstream gaps can be almost flat-topped. The apparatus will be completed in the fall of 1987. The experiment has been completed through section "C" as shown in the photograph presented in Fig. 3. At this writing we are in the process of installing sections "D" and "E" and expect to begin experiments with these sections in place in May 1987.

Diagnostics

As shown in Fig. 1, the induction accelerator units are placed in groups of four, followed by a station that allows pumping and diagnostic access to the beams. The accelerating voltages are monitored with a resistive divider placed across each accelerating gap. Our primary beam diagnostics are arrays of four biased Faraday cups for current measurements. These have rise times less than 0.1 μs and are remotely inserted into the beams as required. We also use arrays of four capacitive pickups which measure the line charge density of the beams and have the advantage of being non-intercepting. The rise time of these is limited by the transit time of the beam through the pickup which, for cesium, can be as long as 0.3 μs. Emittance measurements employ the two-slit method; the detectors are small Faraday cups placed behind the downstream slits. Beam size measurements are made with parallel wire arrays called "Harps" that emit secondary electrons when struck by the cesium beam. The wires are .25 mm wide and are located .5 mm apart. Finally, at the end of the system, an electrostatic energy analyser is set up to analyse the right-hand beam. The analyser has an energy resolution of 0.5% and can be seen in the photograph of Fig. 3. As more of the MBE-4 apparatus is progressively assembled, the analyzer is moved downstream.

CBB 857-5682

Fig. 2. Photograph of a four-beam electrostatic quadrupole array.

Data are collected by digitizing oscilloscopes that are interfaced to a small computer. The computer transfers data to and from the oscilloscopes and, in addition, runs the SLID program for analysis and interpretation of the experiments. The computer also controls the voltage on the electrostatic energy analyzer during measurements of beam energy, and positions the slits during measurements of beam emittance.

Experimental Results

Experiments on MBE-4 have proceeded one section at a time as the apparatus has been assembled. The status of the experiments was last reported at the Heavy Ion Inertial Fusion Symposium [5] in May 1986 and at the "Beams 86" conference [6] in Kobe, Japan in June 1986. At present the major experimental thrust is to study a so-called "acceleration schedule" in which the current is amplified as $\beta^{2.5}$. The accelerating waveforms that are used in the first twelve gaps are shown in Fig. 4. These were obtained by using the SLID code, experimental observation, and iteration procedure detailed above. Accelerating voltages at gaps 4, 9, and 11 contain components to control the longitudinal space-charge spreading of the beams as well as to accelerate the beams. The waveforms in section "C" (gaps 11-14) were synthesized in such a way that the accelerating voltage seen by beams passing through adjacent gaps was of the correct form to retain the desired self-similar current waveforms. That is, waveforms on adjacent gaps, as opposed to individual gaps, were required to synthesize the self-similar current amplifying acceleration schedule.

Oscillograms of each of the four cesium beams at the entrance to the accelerator and at diagnostic stations 5, 10, and 15 are presented in Fig. 5. These were obtained using four arrays of four Faraday cups. There are some variations in calibration among the 16 cups. By electronically

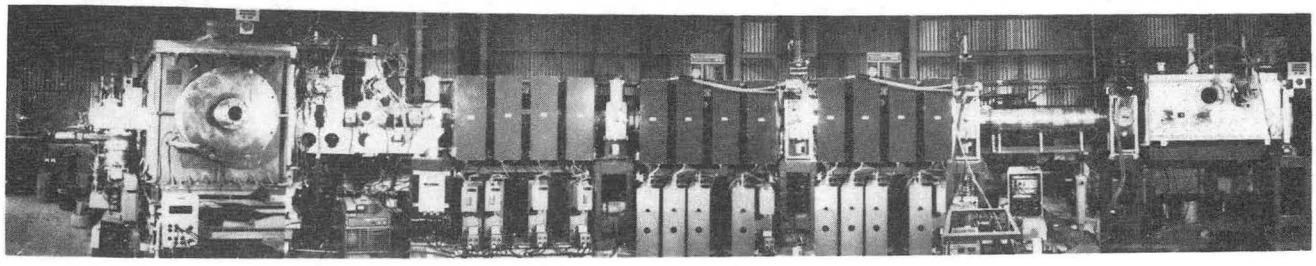

CBB 868-6793A

Fig. 3. Photograph of MBE-4 taken in Nov. 1986.

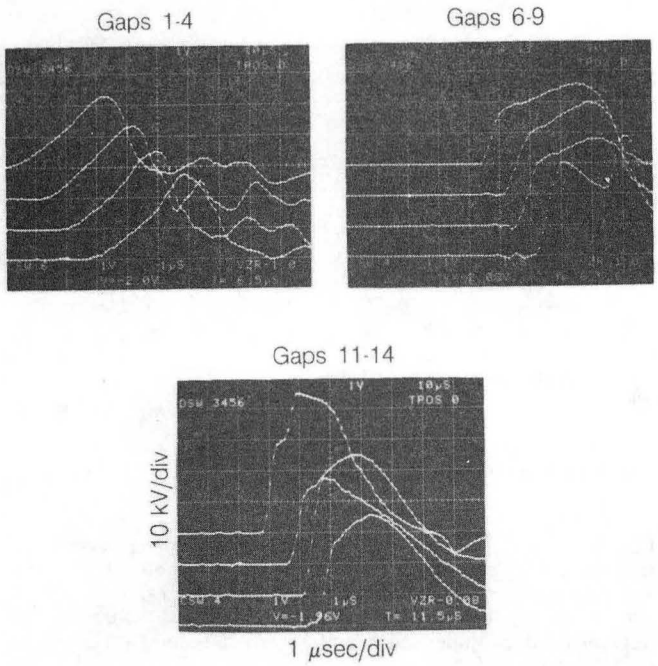

XBL 873-8811

Fig. 4. Oscillograms of the waveforms used in the first 12 accelerating gaps of MBE-4.

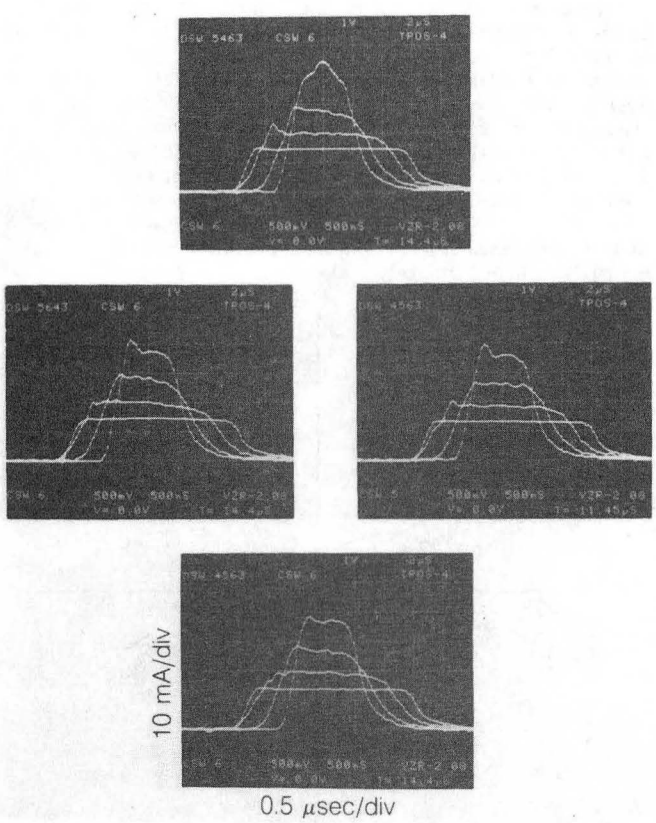

XBL 873-8812

Fig. 5. Cesium beam current wave forms at stations 0, 5, 10, and 15.

integrating the 16 current traces, we determined that the measured charge contained in each beam at each station varies by no more than 5%. For a given beam the charge varies by less that 3% along the length of the apparatus. These variations are of the same order as our experimental error. The small peak on the top beam at station 15 is an artifact due to faulty operation of that particular Faraday cup.

Measurements of the time dependence of the energy of the right hand beam are shown in Fig. 6. In taking these data the analyser was located after section "D" which contained no acceleration. With each firing of the machine, the computer raised the electrostatic analyzing voltage in steps corresponding to approximately one percent of the energy range being scanned. To obtain a beam energy measurement requires the better part of one hour. After recording the data the computer calculates the mean and standard deviations of the detected signal to obtain the beam energy versus time.

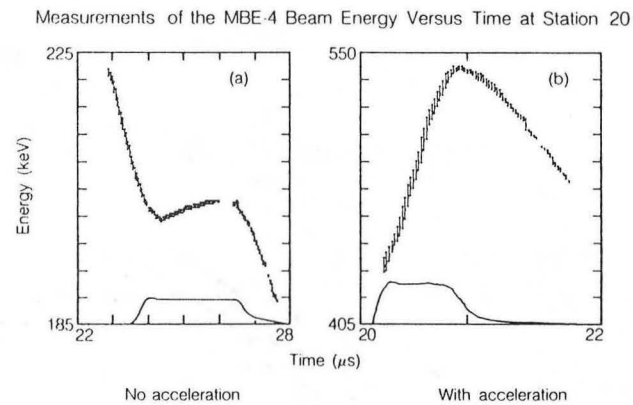

XBL 873-8813

Fig. 6 Measurements of the Beam energy versus time at Station 20. a) Without acceleration, b) With acceleration.

Figure 6a shows the energy variation versus time for a beam drifted through the accelerator from the injector to the analyser without acceleration. As a result the longitudinal space charge fields at the bunch ends were not compensated and the particles at the beam head gain energy from the bunch while the trailing particles lose energy. (An analysis of this physics was done by Faltens, Lee and Rosenblum [7] using experimental data taken from the Single Beam Transport Experiment [8].) The energy of the beam in the main body of the pulse is not exactly constant but shows a slight ramp of about 1.5%.

Figure 6b shows the energy of the MBE-4 beam accelerated by the waveforms in Fig. 4 to an average energy near 500 keV. The normalized beam velocity shear ($\Delta\beta/\beta$) is approximately 10% from head to tail. The down-turn in energy at later times occurs after the main body of the pulse and is associated with particles trailing behind that constitute a small fraction of the total. An aperture located at station 15 was used to greatly reduce the beam current and longitudinal space-charge effects as the beam passed through the drift section "D". However, for the accelerated beam, the beam velocity tilt at the end of the accelerator results in additional pulse shortening and current amplification before the beam energy is measured.

The SLID code was used to calculate the expected current and energy profiles at stations 0, 5, 10, and 15, where the diagnostics are located The results of these calculations are presented in Fig. 7. The SLID code was run in the analysis mode wherein the measured accelerator waveforms presented in Fig. 4 and the beam current and energy at the entrance to the accelerator were provided as inputs. SLID calculations of the energy at the position of the energy analyser are included in Fig. 6 for comparison.

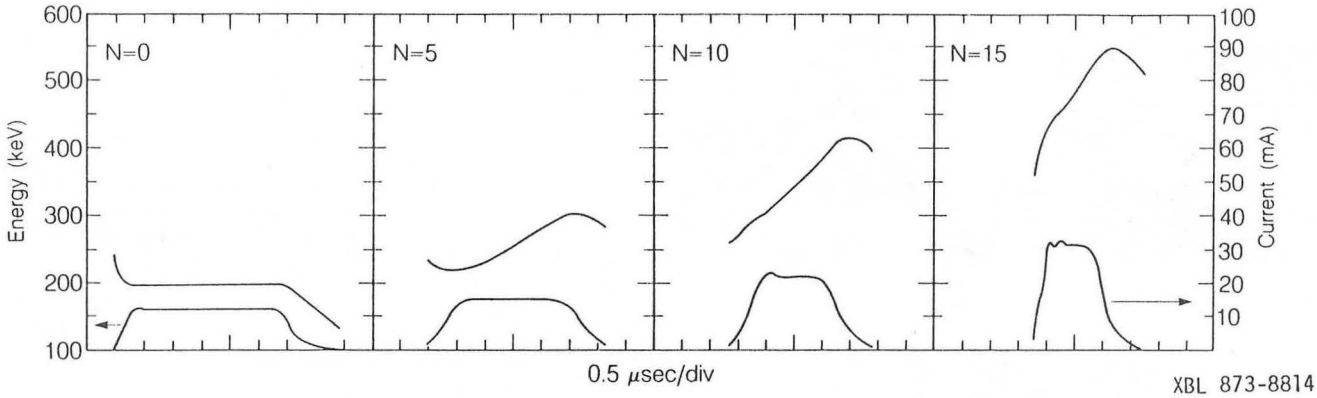

Fig 7. SLID Calculations of the MBE-4 current waveforms and energy at stations 0, 5, 10, and 15.

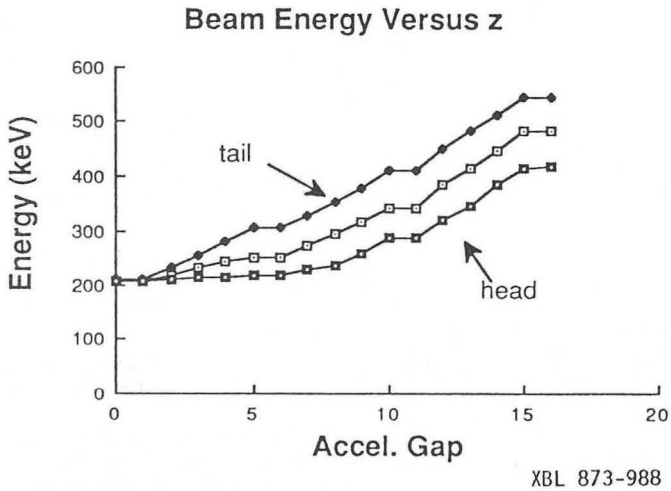

Fig. 8 Plots of the tail, center, and head energy of the MBE-4 beams as calculated by the SLID code from experimental data.

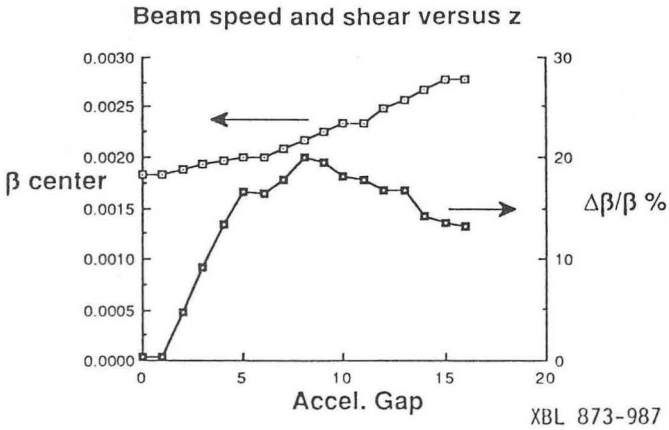

Fig. 9 Beam speed at pulse center and normalized velocity shear of the MBE-4 beams in the accelerator.

Further analysis of the experimental operation of MBE-4 obtained with the SLID code is presented in Figs. 8 and 9. Figure 8 shows calculations of the energy of the beam tail, center, and head for the above experimental conditions. The energy variation at station 15 can be compared with the measurements of beam energy shown in Fig. 6. Figure 9 shows the variation of the beam speed and the velocity shear, $\Delta\beta/\beta$, along the accelerator. The velocity shear peaks at 20% at period 7 then falls to 13% at the end of the present apparatus. The absence of acceleration in gaps 5, 10, and 15 is reflected by flat spots on the curves of beam energy versus z in Fig. 8 and beam speed in Fig. 9 at these locations.

Several experiments were performed to study the evolution of the beam emittance with time under acceleration. We measured the emittance of the bottom beam at station 15 at times near the head, center, and tail of the pulse. We also measured the beam emittance at pulse center at the gun exit (M1) and at station 15 with the accelerator turned off. The time window of the measurement is 60-70 ns. Figure 10 shows a plot of the bottom cesium beam in horizontal phase space at station 15. The contours are selected on the basis of amplitude and enclose all points that are greater than, respectively, 5, 10, 20, and 50% of the maximum signal. These data were taken at the time center of the pulse at the instant that the beam energy was approximately 500 keV.

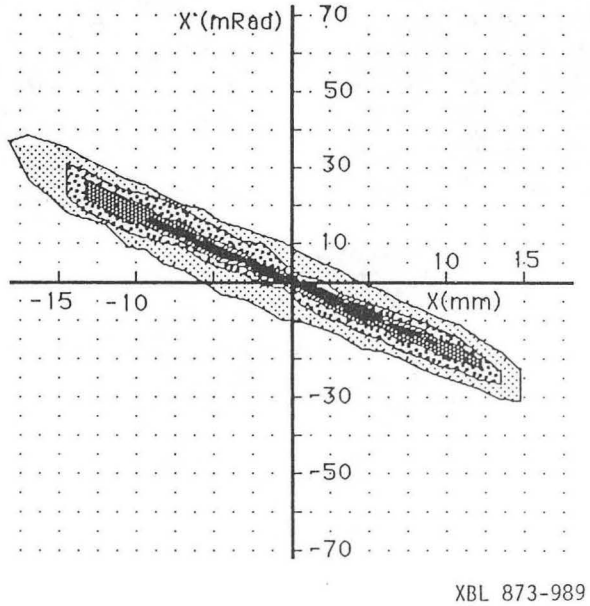

Fig. 10. The bottom cesium beam at station 15 in horizontal phase space. Mean x = -1.4 mm; rms x = 7.6mm; Mean x' = 2.6 mR; Rms x' = 13.9 mR; beam offset, 1.4 mm in x, 2.6 mR in x;. Rms emittance = 20.1 mm-mR with 95% of the particles.

The computer code EPLOT is used to calculate the r.m.s. emittance. We define the rms emittance as

$$\epsilon_{rms} = \left(\langle x^2\rangle\langle x'^2\rangle - \langle xx'\rangle^2\right)^{1/2} \qquad (1)$$

where $\langle x\rangle$ and $\langle x'\rangle$ are, respectively, the r.m.s. beam size and the r.m.s. transverse velocity normalized to the parallel velocity. The parameter $\langle xx'\rangle$ is the rms mean product of the beam size and normalized parallel velocity. The normalized emittance is defined as $4\beta\epsilon_{rms}$ in the computations reported here.

Results are presented in Table I. The experimental error in these data is considerable due to electrical noise generated by the pulsers firing and the data is not believed accurate to better than 20%. These results suggest that the normalized emittance remains constant under acceleration as expected and that there is no evidence of transverse emittance growth. Nevertheless, more experiments are required before we can be confident of this conclusion. We are in the process of developing the coding that will enable us to measure beam emittance simultaneously at several positions within the pulse instead of at one time; this will greatly shorten the required experimental time.

Table I
Beam Emittance Measurements

pulse	Energy (keV)	rms Emit. (mm-mR)	norm. Emit. (mm-mR)	Comment
center	200	31	0.22	M1 Gun exit
center	200	29	0.21	15 Accel. off
head	450	26	0.28	15 Accel. on
center	500	20	0.23	15 Accel. on
center	500	21	0.24	15 Accel. on
tail	550	21	0.25	15 Accel. on

Discussion

We have accelerated four parallel space-charge dominated cesium ion beams from 0.2 MV to nearly 0.6 MV with a current amplification of 2.8 in the partially complete MBE-4 apparatus. The experiments are in excellent agreement with our theoretical acceleration model.

The acceleration schedule is one in which the current waveforms grow in amplitude and decrease in pulse duration in a self-similar or self-replicating way with acceleration distance. Aside from small fluctuations, generated by small errors in the acceleration waveforms, the experimental current waveforms are self-replicating. The acceleration errors are mostly corrected by "trim" pulsers located at approximately every fourth accelerating gap. These are also used to control space charge spreading of the ends of the beam bunches. Comparisons of the measurements of the actual accelerating waveforms with those calculated theoretically are used to derive small corrections to the design of the pulsers that provide the accelerating waveforms for subsequent gaps.

Preliminary measurements of the beam emittance versus position in the pulse, after acceleration of the cesium beams from 200 keV to nearly 600 keV, have revealed no unpleasant surprises. The normalized emittance appears to remain constant as expected. A more thorough experimental study will be made when the MBE-4 apparatus is completed.

Current amplification with acceleration in a linac is only possible for beams moving non-relativistically. In order to overcome the effects of space charge and control the bunch length within the accelerator, one must precisely control of the longitudinal acceleration fields seen by the beam. Small acceleration errors, if uncorrected, lead to growing current fluctuations that result in beam spill or momentum spread. We have been successful in controlling the consequences of unavoidable small errors with the use of the Kim-Smith longitudinal acceleration model as incorporated into the SLID computer code. Future experiments will give a clearer picture of the importance of current fluctuations in the operation of an ion induction linac and how effectively they may be controlled.

Acknowledgments

We wish to acknowledge the excellent engineering support provided by C. Pike, D. Vanecek, D. Gough and their crews in fabricating and assembling the apparatus.

References

[1] C.H. Kim and L. Smith, Part. Accel. 85, pp. 101-113, (1985).

[2] C.H. Kim, V.O. Brady, T.J. Fessenden, D.L. Judd, and L.J. Laslett, IEEE Trans. on Nuc. Sci., NS-32, p. 3190, (1985).

[3] R.T. Avery, C.S. Chavis, T.J. Fessenden, D.E. Gough, T.F. Henderson, D. Keefe, J.R. Meneghetti, C.D. Pike, D.L. Vanecek, and A.I. Warwick, IEEE Trans. on Nuc. Sci., NS-32, p. 3187, (1985).

[4] A.I. Warwick, D. Vanecek, and O. Fredriksson, IEEE Trans. on Nuc. Sci., NS-32, p. 3196, (1985).

[5] D. Gough, D. Brodzik, A. Faltens, C. Pike, and J. Stoker, "Pulsers for the Induction Linac Experiment, MBE-4", this conference.

[6] T.J. Fessenden, D.L. Judd, D. Keefe, C. Kim, L.J. Laslett, L. Smith, and A.I. Warwick, AIP Conf. Proc. 152, Heavy Ion Inertial Fusion, Wash. D.C., p. 145, (1986).

[7] T.J. Fessenden, R.T. Avery, D.A. Brodzik, C.S. Chavis, A. Faltens, D.E. Gough, T.F. Henderson, D.L. Judd, D. Keefe, C. Kim, L.J. Laslett, J.R. Meneghetti, C.D. Pike, L. Smith, D.L. Vanecek, and A.I. Warwick, "MBE-4: An Induction Linac Experiment for Heavy Ion Fusion", Sixth International Conference on High-Power Particle Beams, Kobe, Japan, June 9-12, 1986.

[8] A. Faltens, E.P. Lee, and S.S. Rosenblum, "Beam End Erosion", Submitted to J.A.P. also LBL report LBL-19508 January 1986.

[9] W. Chupp, A. Faltens, E.C. Hartwig, D. Keefe, C.H. Kim, L.J. Laslett, R. Nemetz, C. Pike, S.S. Rosenblum, J. Shiloh, L. Smith, M. Tiefenback, and D. Vanecek, IEEE Trans. Nucl. Sci., NS-30, 2549 (1983).

PULSERS FOR THE INDUCTION LINAC EXPERIMENT, MBE-4*

D. Gough, D. Brodzik, A. Faltens, C. Pike, and J. Stoker

Lawrence Berkeley Laboratory
University of California
Berkeley, California 94720

Summary

The MBE-4 proof-of-principle experiment uses an induction linac to accelerate four Cs+ beams from injection at 200 kV to almost 1MV. When completed in the summer of 1987 it will be 17.2 meters long and have 24 acceleration gaps and 6 diagnostic gaps. Careful tailoring of the accelerating voltage waveforms at each gap is required to accelerate the beam, amplify the current and provide longitudinal focusing. The ideal voltage waveforms required at the first 4 gaps are almost triangular with an amplitude of about 20 kV and an approximate width of 3 μsec, becoming flatter and shorter with an amplitude of 30 kV at subsequent gaps as the beam current increases and the pulse width narrows. These waveforms [1] are shown in Fig. 1. Pulser voltage waveforms at each gap are adjusted in both amplitude and firing time in conjunction with beam experiments to determine the required voltage waveforms of the subsequent pulsers. Existing cores and previous experience with thyratron pulsers provided the basis for the pulsers for the first half of the machine. During this fabrication period, additional cores and spark gap pulsers capable of generating higher voltages than the thyratron pulsers became available and a combination of both types of pulser will be used to complete the apparatus.

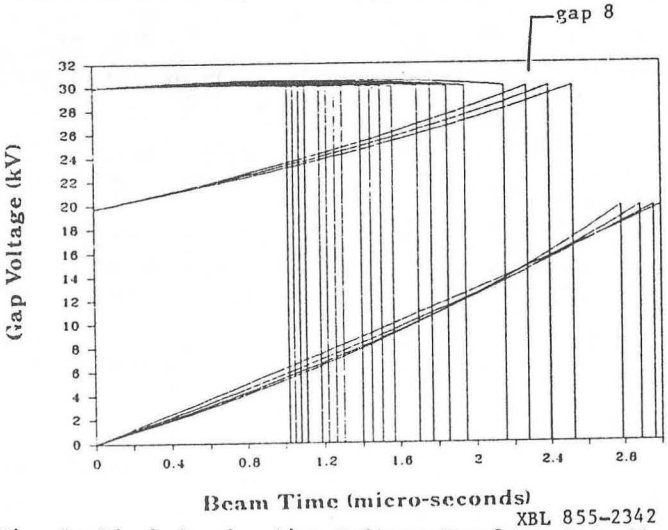

XBL 855-2342

Fig. 1 Ideal Accelerating Voltage Waveforms for all 24 Gaps

Introduction

MBE-4, when complete, will have 24 accelerating gaps. The initial complement of available cores consisted of 92 nickel-iron tape wound cores [2] capable of 6.8 mVsec/core and 26 silicon steel tape wound cores [3] capable of 24 mVsec/core. Groups of these cores were used with an appropriate number of thyratron pulsers to provide the necessary accelerating voltage waveforms at the first eight gaps together with the required voltage waveforms which provide the longitudinal control of the beam ends. Additional silicon steel tape wound cores capable of nominally 60 mVsec/core became available and some of these were used in conjunction with the existing cores to provide the necessary accelerating voltage waveforms at the next four gaps (#11 - 14) using thyratron pulsers. Four different pulser circuit types were identified as possible solutions for generating the required waveforms. These pulsers are typically identified by their generated voltage waveforms which are either parabolic, (1-cos ωt), trapezoidal, or capacitor discharge. Basic circuits were established to generate the required voltage wave-forms using thyratron pulsers and at the same time basic performance characteristics were established for the cores. In order to generate the parabolic waveform it was necessary to connect a resistor in parallel with the core so that it dominated the load resistance. This introduced additional circuit losses that are undesirable, therefore this circuit configuration has not been pursued. The computer program Spice [4], together with some basic characteristics for each type of core, has been used to predict the performance of any proposed circuit configuration. This has enabled the number and type of thyratron pulser circuits required for each gap to be defined so that they generate the specified voltage waveforms. A standard pulser package, including reset, was established which could operate at a maximum voltage of 30 kV, with the pulser output waveform characteristics being determined by the pulse-forming network installed internally in the designated area.

A spark gap pulser built by Ford Laboratories was modified to operate in conjunction with four of the nominal 60 mVsec cores. This pulser arrangement is used at two of the acceleration gaps to provide most of the acceleration voltage specified for four of the gaps. Corrections to the generated acceleration voltage waveform and the voltage waveforms required to provide longitudinal control of the beam ends are obtained using four thyratron pulsers.

Thyratron Pulser Development

An analytically derived model for magnetic induction cores [5] is, in its simplest form, a resistance in parallel with an inductance and this is used with the other appropriate circuit elements to predict pulser performance. The values of resistance and inductance used to represent a specific core is voltage-level dependent; core package measurements were made to determine these resistance values. An initial value of inductance was calculated and used with the appropriate core resistance equivalence at specific charge voltages to generate computed voltage and current waveforms. The inductance value was modified using the measured current waveform as reference until the computed waveform matched the measured waveform up to saturation level. This was carried out for all the different core packages to establish the core model [6] for any core/circuit combination.

The computed and measured characteristics for a

*This work was supported by the Office of Energy Research, Office of Basic Energy Sciences, U.S. Dept. of Energy under Contract No. DE-AC03-76SF00098.

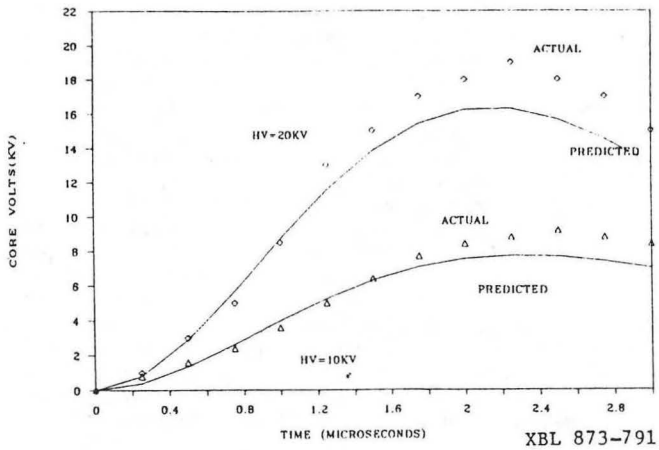

Fig. 2 Computer predicted and measured core voltage for a core package containing two 24 mVsec silicon steel cores and a (1-cos ωt) pulser at a charge voltage of 10 kV and 20 kV.

core package containing two 24 mVsec silicon steel cores and a (1-cos ωt) pulser at charge voltages of 10 kV and 20 kV are shown in Fig. 2. All the (1-cos ωt) and capacitor discharge circuit arrangements used on MBE-4 were evaluated in the same way and showed reasonable agreement between the measured and computed waveforms. The computed and measured results for a trapezoidal waveform pulser using a core package containing two 24 mVsec silicon steel cores has been demonstrated. This circuit configuration has not yet been used on MBE4 because it is not compatible with an optimized pulser arrangement for the required accelerating voltage waveform schedule.

Selection of the core package arrangements, type of pulsers and number of pulser circuits is carried out by matching these to the accelerating voltage specified for a given gap. The number of pulser circuits is kept to a minimum and the core package usage is maximized. Computed voltage waveforms, within the limits of the standard thyratron pulser, for each of the proposed pulser circuits are generated. A composite of these waveforms is also pro-

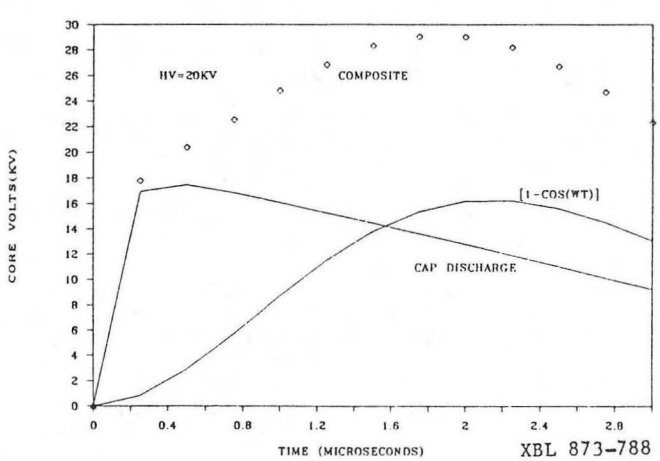

Fig. 3 Predicted individual and composite voltage waveforms for a (1-cos ωt) pulser and a capacitor discharge pulser for a charging voltage of 20 kV each. The core package for each pulser contains two 24 mVsec silicon steel cores.

duced so that it can be compared with the specified waveform. A capacitor discharge pulser and a (1-cos ωt) pulser each using a core package containing two 24 mV sec silicon steel cores was proposed for gap 8 and the computer predicted waveforms are shown in Fig. 3. This can be compared to the ideal accelerating voltage waveform for gap 8 as shown in Fig. 1.

Two pulsers are normally provided at each gap with additional pulsers being provided at the gaps requiring more complex waveforms. With the capability to control the pulser charge voltage and the trigger time to 10 nsec, it has been possible to minimize the error between the calculated and generated acceleration voltage waveforms. The voltage specified for gap 11 was considered complex and a considerable amount of flexibility was requested. Computer waveform simulation was carried out and from this a four pulser configuration was selected. The ability of this group of pulsers to match the calculated acceleration voltage waveform, which is based on the measured performance at the previous gap, for gap 11 is shown in Fig. 4. [7]

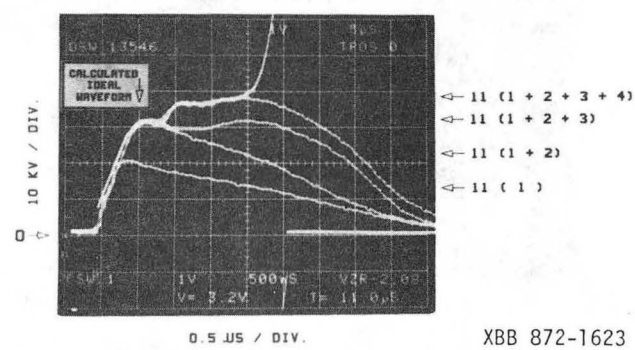

Fig. 4 Comparison of the calculated ideal voltage waveform with the actual composite voltage waveform at gap 11 using four thyratron pulsers.

Spark-Gap Pulser Development

In the spring of 1986 we learned that a project to build an electron induction linac by Ford Laboratories had been discontinued. We then purchased enough of their fabricated silicon steel cores to complete MBE-4, and embarked on a study of their pulser design to see if their excess pulsers could be usefully incorporated in MBE-4. This, indeed, proved to be the case but at the cost of minor modifications to the planned accelerating schedule in the last half of MBE-4. It was pleasing to find that the induction linac design proved flexible enough to accommodate a rather different core arrangement, and quite a different pulser design. The incorporation of the new pulsers, switched by spark-gaps rather than thyratrons, gives a broader base to our pulser technology development.

The results of these tests indicated that the desired flat waveforms in the high energy end of the accelerator could be approximated by the waveform in Fig. 5, augmented by low amplitude (1-cos ωt) pulsers. Whereas the initial design of MBE-4 was based on a maximum voltage of 30 kV per gap and one or more pulsers per gap to obtain the voltage, the new design is 60 kV across each of two adjacent gaps, all driven by one higher power pulser. To achieve this, 4 cores are driven in a series parallel configuration as shown in Fig. 7.

Without correcting networks, the core voltage is a monotonically decreasing function of time as the pulser capacitors are discharged. To flatten the voltage pulse, we added a small series inductance to the existing self inductances of the capacitors, spark gap, and wiring, to obtain a 2:1 voltage divider between the core impedance and the rest of the circuit. Then, to counteract the pulse droop, we added across each of the cores an LC circuit whose function is to take some energy out of the main energy storage capacitor at the beginning of the pulse, and put it into the core near the end of the pulse.

By pulsing the induction cores from remanent B field to saturation in both directions, we found that a typical core has: B_s = 13.5 kG, B_r = 11.2 kG, I_r > 250 Amps, where B_s is the saturation flux density, B_r is the remanent flux density, and I_r is the current required to slowly reset the core. The radial packing fraction, f, which is the ratio of core lamination thickness divided by the lamination plus insulation thickness, was measured as 0.8. Combining these values with the cross sectional area, A_c, of the 11" x 4" core results in an available flux change, $\phi = (B_r + B_s)fA_c$, of 54 mVsec, the usable fraction of which is determined by the core saturation characteristics and the drive circuit to be about 80% for the 1.4 μsec pulse in Fig. 5. The pulse excitation current, or "step" for these cores is about 1 kA, after which the core current shows a saturation wave-like linear increase up to about the 4 kA level. With the aid of this preliminary data the circuit shown in Fig. 7 was constructed and resulted in the voltage and current waveforms shown in Figs. 5 and 6 respectively. A good discussion on pulse magnetization is found in Chapter 15 of Reference [8].

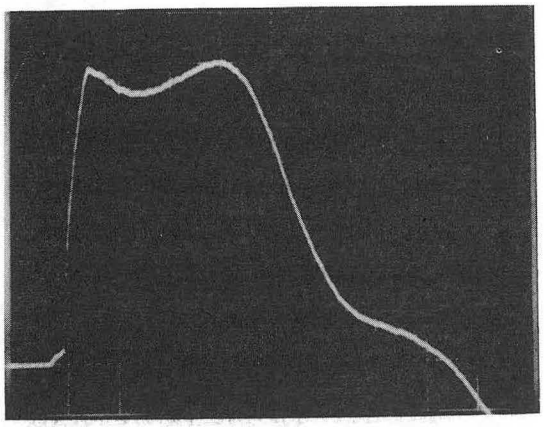

XBB 872-1624

Fig. 5 The accelerating voltage appearing across each of the four induction cores driven by one modulator.

Vert. scale: 5 kV/div. Horz. scale: 500 ns/div.

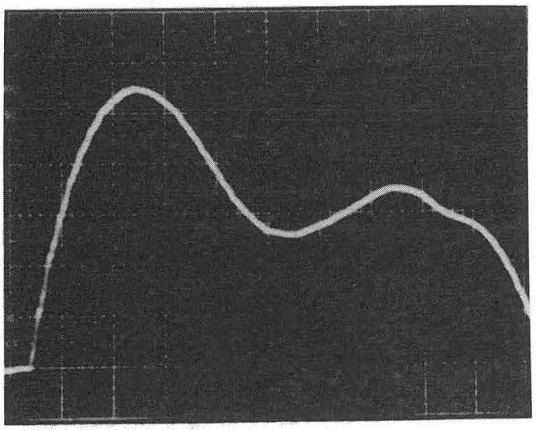

XBB 872-1625

Fig. 6 Modulator output current for the voltage pulse in Fig. 5. As the core enters saturation, near the center of the picture, most of the current is being supplied by the correcting network, whereas at the beginning of the pulse much of the modulator current is going into the correcting network.

Vert. scale: 600 A/div. Horz. scale: 500 ns/div.

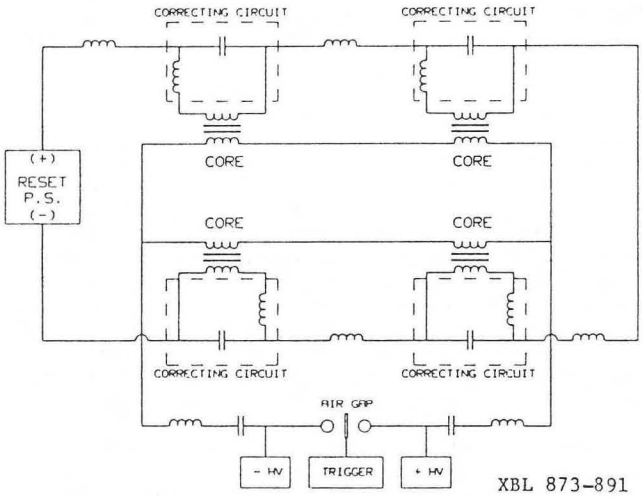

XBL 873-891

Fig. 7 The spark gap pulser circuit

References

1. C.H. Kim, V.O. Brady, T.J. Fessenden, D.L. Judd, and L.J. Laslett, IEEE Trans. Nuc. Sci., Vol. NS-32, No. 5, p. 3190.

2. S.D. Winter, R.W. Kuenning, and G.G. Berg, IEEE Trans. on Mag., MAG-61, p. 41, 1970.

3. A.Faltens, M. Firth, D. Keefe, and S.S. Rosenblum, IEEE Trans. Nuc. Sci., Vol. NS-30, p. 3669, 1983.

4. D.O. Pederson, Spice Version 2G.6, University of California, Berkeley.

5. T.J. Fessenden, D. Keefe, C. Kim, H. Meuth, and A. Warwick, Internal Technical Note, HIFAR Note-48, Lawrence Berkeley Laboratory.

6. D.E. Gough and D. Brodzik, IEEE Conf. of the 17th Pulser Modulator Symposium, June 1986. p. 47.

7. T.J. Fessenden, "The LBL Multiple Beam Experiments", elsewhere in these Proceedings.

8. Pulse Generators, Glasoe and Lebacqz, McGraw-Hill, 1948 and Dover, New York, 1965.

HIF INSULATOR FAILURE

Kurt Kennedy

MBE-4 high voltage feed-thru insulators were made by centrifugally casting a glass in a cast iron mold. At the same time a thin metal ring is embedded in the molten glass. This ring is used to weld the insulator to a vacuum system. These metal ends are made of 430Ti stainless steel and are shaped by spinning.

Several of the insulators have developed vacuum leaks near where the insulator was welded to the vacuum system. This style of insulator had its weld made in the thin metal that had been deformed by spinning.

A micrograph of the weld is shown in Figs. 1 and 2. Figure 1 is unetched and shows grain boundary delineation and that some grain has fallen out. Figure 2 shows the same area after etch with more grains missing. The results of an X-ray microprobe of the weld area are shown in Fig. 3. The grain interior shows only iron and chromium but the titanium, which is in 430 Ti stainless, was absent. The grain boundary is rich in both titanium and sulfur.

It appears that sulfur may have been introduced in the spinning process. During the long heat treatment used in processing the insulators, the sulfur combined with titanium to form Titanium Sulfide in the metal grain boundaries the titanium sulfide which is brittle formed a path for a vacuum leak during the subsequent welding of the part.

A spun ring of 430 Ti stainless, similar to those used in insulator, was analyzed for gross sulfur by normal chemical methods and no sulfur was found. As an experiment, a piece of this ring was annealed at 900°C for 5 hours and welded as in the failed part. Figure 4 shows a micrograph of the welded and unwelded region of this part. The welded area shows the defective grain boundary as found in the failed part but not to the extent of grain falling out.

The failure of the HIF insulators has only been associated with welds made on spun deformed metal. The grain boundaries of the failed welds contain high levels of sulfur. Sulfurized oil is a common lubricate used in spinning. The failure to totally replicate the physical loss of metal grains in the experimental piece is disturbing but the spinning may have had a different history than the failed part.

The weld failure in the HIF insulators appears to be remediable by: (1) Moving the weld from the deformed area of the spun ring; (2) Find a spinning method that does not compromise welding.

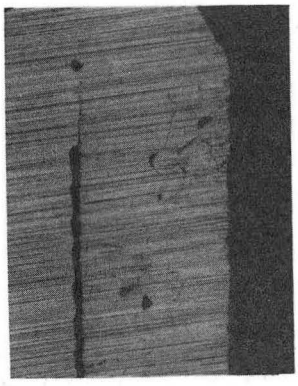

XBB 874-2630

Fig. 1

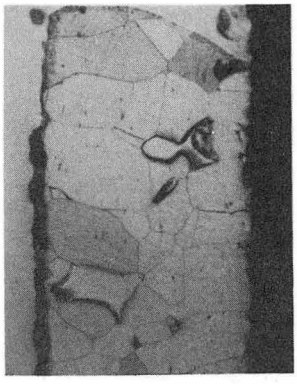

XBB 874-2631

Fig. 2

Figure 3
Grain Boundary

Element & Line	Weight Percent	Atomic Percent	Precision 2 Sigma	K-Ratio	Iter
CR KA	20.39	21.37	0.86	0.2333	
FE KA	80.58	78.63	2.10	0.7667	2

Grain Boundary

Element & Line	Weight Percent	Atomic Percent	Precision 2 Sigma	K-Ratio	Iter
S KA	6.52	10.09	0.43	0.0458	
TI KA	5.92	6.14	0.41	0.0602	
CR KA	19.58	18.70	0.82	0.2094	
FE KA	72.20	64.20	1.88	0.6749	
CO KA	1.03	0.87	0.97	0.0096	3

XBB 874-2632

welded

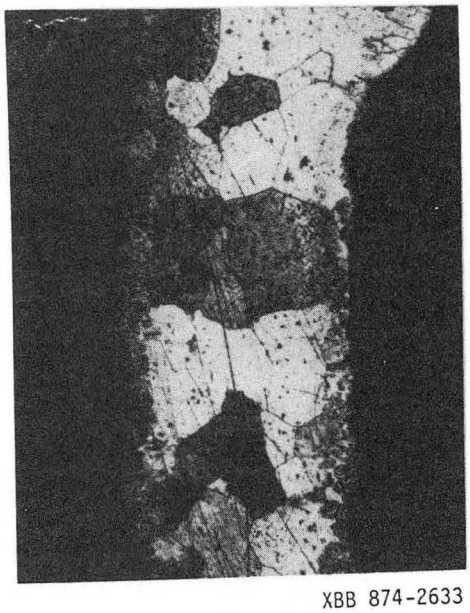

XBB 874-2633

unwelded

Fig. 4.

EXPERIMENTAL MEASUREMENT OF EMITTANCE GROWTH IN MISMATCHED SPACE-CHARGE-DOMINATED BEAMS*

M. G. Tiefenback†
Lawrence Berkeley Laboratory
University of California
Berkeley, California 94720

Abstract

Using the Single Beam Transport Experiment (SBTE) at LBL, we have measured the emittance of a well-matched 4.6-mA beam of 122-keV Cs^+ to be conserved from injection into through exit from an 80-lens segment of the AG focussing channel. We then mismatched the beam into the same channel such that the maximum (minimum) radius of the beam at the midplane between lenses was about 1.5 (0.5) times the former value. We caused mismatches in the envelope of the beam in both transverse dimensions (labeled a and b) in modes both symmetric ($\delta a = \delta b$) and antisymmetric ($\delta a = -\delta b$). We found the mismatch amplitude to decay during the beam transit through the channel for both modes of mismatch, although more so for the antisymmetric mode. We also found the emittance of the symmetrically mismatched beam to be the same as for the matched beam, while the emittance of the antisymmetrically mismatched beam grew by as much as a factor of four over that for the matched beam.

Introduction

Because of the inevitable spread in betatron frequency of the particles in a beam, the particles will eventually "phase-mix" and forget their original neighbors in betatron phase. In the zero-current limit, for a beam that is either misaligned or mismatched within its channel, the beam will eventually diffuse so that its radius is equal to the maximum excursion of the particles of which it is composed.

We expect the same phenomenon to occur within space-charge-dominated beams, although the final radius of the beam will not be determined solely by the initial mismatch or misalignment amplitude, but also by the space-charge self-energy of the beam.

From perturbation of the equations for the envelope of a beam in two transverse dimensions (see, for example, refs. 1 and 2, which we label a and b), we obtain in the limit of continuous focussing, we obtain the following phase advance rates ("wave-numbers," in essence) for the eigenmodes of oscillation:

$$k_{\pm}^2 = \begin{cases} 2\sigma_0^2 + 2\sigma^2, & \delta a = \delta b \\ \sigma_0^2 + 3\sigma^2, & \delta a = -\delta b \end{cases} \qquad (1)$$

where σ_0 is the phase advance per arbitrary length for a single particle in the channel and σ is the net phase advance for a particle under the influence of the self-field of a beam. In the low-temperature limit ($\sigma \to 0$) we see that $k_+ \to \sqrt{2}\sigma_0$ (symmetric mismatch) and $k_- \to \sigma_0$ (antisymmetric mismatch). The symmetric mode frequency is the higher of the two because the space-charge density is affected by this oscillation and not by the antisymmetric mode. We will compare these values with our data below.

*This work was supported by the Office of Energy Research, Office of Basic Energy Sciences, U.S. Dept. of Energy under Contract No. DE-AC03-76SF00098.

†Now at Pulse Sciences, San Leandro, CA.

Method

We used a 4.6-mA beam of 122-keV Cs^+ ions with a normalized emittance of $0.7\times10^{-7}\,\pi$ meter radians for our measurements. We matched the beam into the quadrupole channel of the SBTE by tuning the first five lenses of the channel (M1--M5) [3,4]. The channel was set so that $\sigma_0 = 60°$ (per focussing period), which resulted in a matched beam radius at the midplane between lenses of R_0 = 10 mm. We also tuned the matching lenses to mismatch the beam in the succeeding FODO lattice. In one experiment, the adjustment caused a purely symmetric mismatch. In the other a purely antisymmetric mismatch was created. In each case the maximum (minimum) radius between quadrupoles reached 1.5 R_0 (0.5 R_0).

Our emittance measurements were made using pairs of 0.010-inch-wide slits spaced 6 inches apart longitudinally. We have defined our "emittance" in terms of the measured phase space distribution in the following way: We delete the low-level measurements until the beam current represented by the sum of the remaining points drops to 95% of the original total. The emittance is then $4\beta\gamma$ times the RMS emittance of the subset of the data:

$$\varepsilon = 4\beta\gamma \sqrt{\langle x^2\rangle\langle x'^2\rangle - \langle xx'\rangle^2}\ .$$

Results

The beam radius (defined as twice the RMS radius of the beam) near the injection and exit of the periodic channel is shown in Table 1 for these three sets of initial conditions.

For the beam parameters given above and for σ_0 = 60° we calculate $\sigma \simeq 8°$ from the solution to the envelope equations. Thus $k_+ \simeq 86°$ and $k_- \simeq 62°$. The envelope data for the symmetric mode show that the minimum occurs

Table 1: Summary of beam radius data (in mm) for an approximately matched beam (Case I), a symmetrically mismatched beam (Case II), and an antisymetrically mismatched beam (Case III). In the two mismatched cases, the maximum amplitude of the beam was about 16 mm.

	Case I		Case II		Case III	
	R_V	R_H	R_V	R_H	R_V	R_H
M5	10.5	11.9	14.2	14.6	9.2	13.8
Q1	9.4	12.2	~ 14	14.8	3.8	15.3
Q5	10.0	8.1	5.2	6.8	15.1	8.5
Q7	11.9	10.7	12.9	12.1	15.8	4.0
Q9	10.3	10.7	13.6	15.0	9.8	9.2
Q73	10.8	9.4	11.5	11.5	12.0	10.7
Q75	10.0	9.7	10.2	11.3	9.9	11.3
Q77	8.6	9.0	7.33	7.7	10.2	11.8
Q79	-	9.9	-	9.9	-	11.7

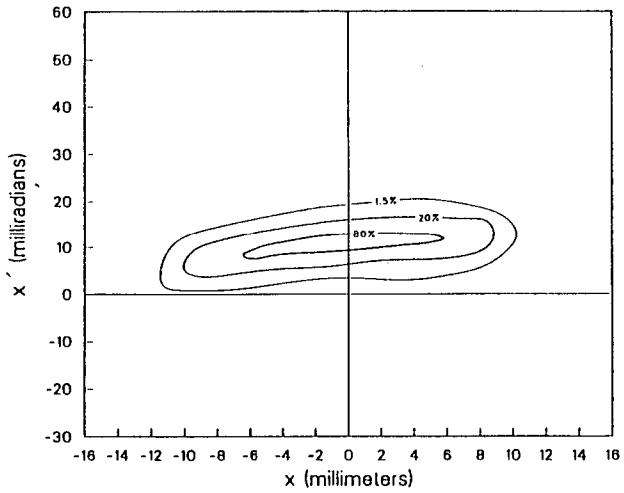

XCG 873-6806

1A

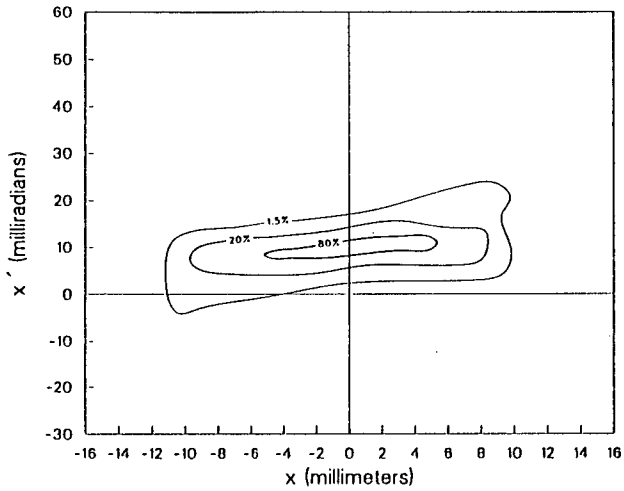

XCG 873-6804

1B

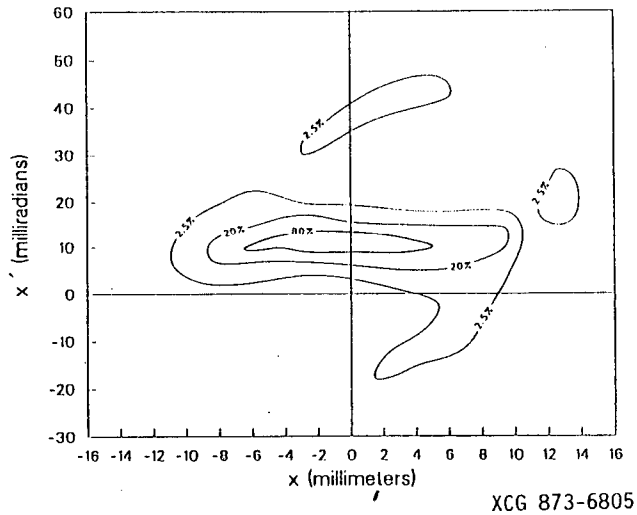

XCG 873-6805

1C

Fig. 1. Phase space contours for A) the matched beam, B) the symmetrically mismatched beam, and C) the antisymmetrically mismatched beam, transformed to suppress the overall focussing of the beam and make the phase ellipses approximately upright. The contour levels for A) and B) are for 1.5%, 20%, and 80% of the peak density at the center of the beam. The lowest contour level for C) was chosen as 2.5% of the peak level in order to show the gradient in phase space density and give a sense of the direction of particle diffusion in phase space. At the 1.5% level, the clockwise-pointed tails in phase space have encircled the body of the distribution, enclosing two regions of very low particle density. We expect that the 4-dimensional phase space density is conserved, while the 2-dimensional projected density measured experimentally is not conserved.

Table 2: Emittances of the beam for the various cases at the end of the transport channel (Q80) and for the most intense 95% of the distribution (to eliminate low-level data points and avoid heavy weighting of the distribution tails by the RMS emittance calculation).

Case I	Case II	Case III
0.67×10^{-7}	0.68×10^{-7}	2.94×10^{-7}

about 2 periods (4 lenses) after the maximum, so we would estimate $k_+ \simeq 90°$. Similarly, the antisymmetric mode shows an interchange of radius values over 3 periods, so we measure $k_- \simeq 60°$. These numbers are in close agreement with the values calculated from Eq. (1). The amplitudes of oscillation damp between injection (Q1) and exit (Q80), although the damping is less pronounced for the symmetrically mismatched beam. The measured emittance of the beam at Q80 (80 lenses downstream from the matching lenses, shown in Table 2) is unchanged for the symmetric mismatch with respect to the matched beam, but the emittance of the antisymmetrically mismatched beam is 4 times as great as for the matched beam.

The phase space contours shown in Figs. 1A)-C) show the marked difference between the antisymmetrically mismatched beam and the others. The matched beam in A) and the symmetrically mismatched beam in B) are very much alike in distribution. In contrast, a very extensive, but low-level, halo has formed around the beam core in phase space for the antisymmetrically mismatched beam. The lowest contour level in C) was chosen as 2.5% rather than 1.5% to show the gradient in density from the ends of the distribution. It is as if particles are being ejected from the ends of the distribution and wrapping clockwise around the beam. The contour at the 1.5% level (not shown) actually reconnects with the body of the distribution, enclosing void areas. Recall that the 4-d transverse phase space density $\rho(x,y,x',y')$ is expected to be conserved here, while the projected density need not be conserved under the influence of non-linear fields.

We also compare the peak signal level for the three cases to separate the effect of the tails of the distribution on the emittance from that of changes in the core of the distribution. The average of the three adjacent highest values in the distributions was highest for the matched beam, falling to about 95% for the symmetric and 77% for the antisymmetric mismatches. The change in emittance is thus not due solely to the extensive tails of the distribution shown in Fig. 1C.)

We note that the extensive tails of the distribution are only at the level of 2-3% of the peak intensity in the antisymetrically mismatched beam. We measured the phase space distribution at Q35 and found the same structure as that shown in Fig. 3 (including enclosed voids), but the halo was at the level of 1-2% of the peak and the voids were

much cleaner. [Up to this point, the antisymetric mismatch had been generated from the configuration for the matched beam by raising the strength of lens M5 to about 20% above its nominal value. To check the dependence of the emittance growth on the mismatch amplitude, we then set this lens to about 14% above the value for the matched beam, expecting to have an antisymetrically mismatched beam with mismatch amplitude about 2/3 of the original value. When we measured the emittance at Q35 and Q80, we found that the same structure was present as before, but only at the level of 0.5-1% of the peak. The emittance at Q80 was reduced to $1.75 \times 10^{-7}\,\pi$ meter radian, but still well above the value for the matched beam, and the peak intensity was 82% of that for the matched beam.]

Interpretation of the Data

The ideal beam dynamics of the K-V distribution depends delicately upon the linear nature of the beam self-field. Real beams are not so smooth as mathematical beams, and if a space-charge-dominated beam is focused into a very eccentric profile (long in the x-dimension, say), this clumpiness can manifest itself in a large variation of the electric self-field component E_y as a function of x. In the severe antisymetric mismatch we caused in Case III, the beam is very ribbon-like, having an aspect ratio of approximately 4:1. In the case of the symmetric mismatch, the maximum beam aspect ratio remains near the value given by the AG flutter, which is about 1.5:1 for $\sigma_0 = 60°$.

This observation could well explain certain problems in beam matching encountered in the extensive SBTE survey reported elsewhere [3]. There it was noted that it became more difficult to match the beam cleanly to the FODO lattice the further the beam aspect ratio departed from unity.

References

[1] R.L. Gluckstern, "Oscillation Modes in Two Dimensional Beams," in Proceedings of the 1970 Proton Linear Accelerator Conference, FNAL, Batavia, Illinois, 1970, pp. 811-822.

[2] J. Strückmeier and M. Reiser, "Theoretical Studies of Envelope Oscillations and Instabilities of Mismatched Intense Charged-Particle Beams in Periodic Focusing Channels," Particle Accelerators, 15, pp. 227-260, 1984.

[3] Michael G. Tiefenback, "Space-Charge Limits on the Transport of Ion Beams in a Long Alternating Gradient System," Ph.D. Thesis, University of California, Berkeley, HI-FAN-352, LBL-22465, Aug. 1986.

[4] M.G. Tiefenback and D. Keefe, "Measurements of Stability Limits for a Space-Charge-Dominated Ion Beam in a Long A.G. Transport Channel," in Proceedings of the 1985 Particle Accelerator Conference, IEEE Transactions on Nuclear Science, NS-32, 1985, pp. 2483-2485, also LBL-19647.

THE EFFECT OF NONLINEAR FORCES ON COHERENTLY OSCILLATING SPACE-CHARGE-DOMINATED BEAMS*

C.M. Celata
Lawrence Berkeley Laboratory
University of California
Berkeley, California 94720

Abstract

A particle-in-cell computer simulation code has been used to study the transverse dynamics of nonrelativistic misaligned space-charge-dominated coasting beams in an alternating gradient focusing channel. In the presence of nonlinear forces due to dodecapole or octupole imperfections of the focusing fields or to image forces, the transverse rms emittance grows in a beat pattern. Analysis indicates that this emittance dilution is due to the driving of coherent modes of the beam near their resonant frequencies by the nonlinear force. The effects of the dodecapole and images forces can be made to effectively cancel for some boundary conditions, but the mechanism is not understood at this time.

Introduction

The high power density needed on target for a heavy ion fusion reactor implies the need for extremely intense beams. In the parameter range of interest such beams are "space-charge-dominated"--i.e., the space charge forces, rather than the emittance, determine the beam envelope radii. Indeed, about 99% of the focusing field strength is cancelled by the space charge force, giving a space-charge-depression of the betatron frequency to ~ 0.1 of its zero-current value.

The general problem addressed in part by this paper is the question of what phenomena limit the intensity of a coasting beam which can be stably transported without emittance degradation in an alternating gradient focusing channel. This question has been investigated by Hofmann, Laslett, Smith, and Haber[1] for the case where image forces are neglected and no external nonlinearities are present. In that paper it was shown that coherent modes of the beam exist. However, these modes were shown by simulation to be nonlinearly stabilized with negligible emittance growth when $\sigma_0 \leq 80°$,[1,2] where σ_0 is the zero-current value of the betatron phase advance per lattice period for a particle. This was confirmed by experiment.[3]

In this paper we examine the effect of external nonlinear forces and image forces, i.e., the forces due to charge induced on the conductors around the beam, on space-charge-dominated beams. Note that for intense beams the image forces can become of the order of the focusing field forces. As discussed below, no important effect on beam quality is found for beams which are centered in the focusing channel. However, for misaligned beams significant emittance increase is seen for all of the nonlinearities that have been studied.

Emittance Growth Due to Misalignments

We will first consider the effect of forces due to charge induced on nearby conductors, the so-called "image forces", on the beam. We have studied two different boundary conditions: the round conducting pipe concentric with the center of the focusing channel, and the case pictured in Fig. 1, which we shall refer to as the "cylindrical quadrupole" geometry. Figure 1 shows four conducting cylindrical electrostatic quadrupole electrodes surrounding the beam. This models the geometry presently used in the Single Beam Transport Experiment and Multiple Beam Experiment of the Heavy Ion Fusion Program at Lawrence Berkeley Laboratory. Though in the experiments the electrodes occupy only about 60% of the longitudinal space available, we have made the simplifying assumption in the simulation code that the electrodes are present at all longitudinal locations. The error implicit in this assumption is ameliorated by the fact that the beam radius is smaller between electrodes, and therefore image forces are less important. The simulation imposes periodic boundary conditions along the dashed line shown in Fig. 1. This simulates the case of an (infinite) array of beams in a regular array of focusing electrodes. All conductors are assumed by the code to be perfect conductors.

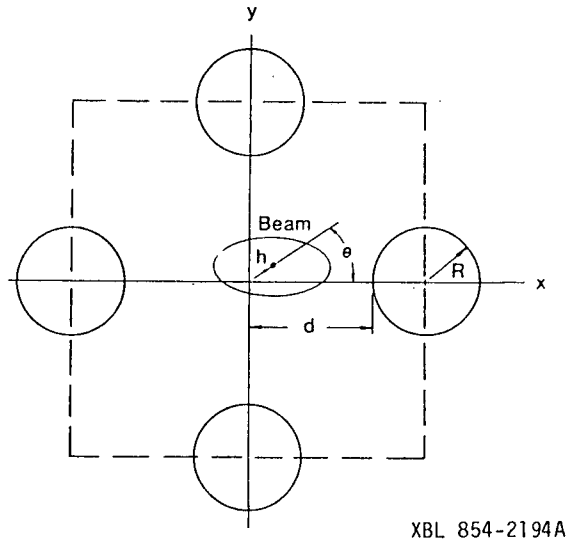

Fig. 1. The geometry of the model, showing the transverse plane, with conducting electrodes (present at all z) and the boundary of the simulation grid (dashed).

The particle-in-cell code used for this study was the code SHIFTXY, written by I. Haber. It is a two dimensional (x-y) nonrelativistic code. Space charge forces are computed self-consistently. For the studies presented in this paper, alternating gradient focusing has been modeled using a thin lens approximation, though the code is capable of calculating for finite-length focusing elements. With only a few exceptions, which will be noted below, the initial distribution function used was gaussian in v_x and v_y, with uniform temperature and density.

For the case of a beam in a square conducting pipe, it was shown by I. Haber[4] that although the shape of the beam is changed, the emittance of a centered beam is unaffected by image forces unless the beam fills more than 85% of the aperture radius. For larger filling factors particle loss occurs. We also observe very little effect on beam emittance for centered beams for any of the nonlinearities studied, until the beam fills most of the aperture. Phase plots for a centered beam in the cylindrical quadrupole geometry, with no external nonlinearities present, are shown in Figs. 2 and 3 for the beam initially and after 19 periods of transport. In this case, where the beam fills 75% of the aperture radius, there is an initial rise in rms emittance by about 8%, followed by a very slow rise of ~ 1.5% per 100 periods.

*This work was supported by the Office of Energy Research, Office of Basic Energy Sciences, U.S. Department of Energy, under Contract No. DE-AC03-76SF-00098.

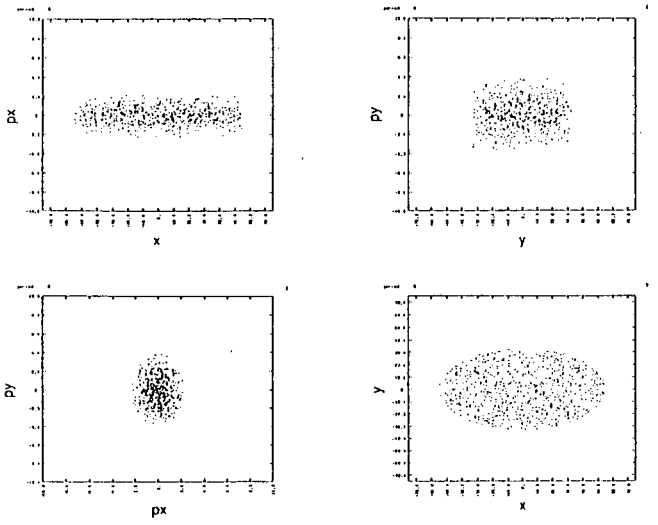

XBL 873-1360

Fig. 2. Phase plots for initial distribution function for centered beam. $\sigma_0 = 60°$, $\sigma = 6°$, rms major radius/distance to electrode surface = 0.375.

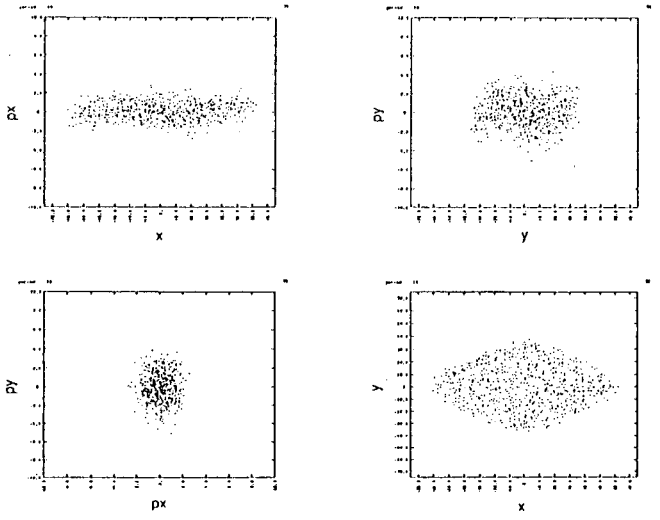

XBL 873-1359

Fig. 3. Phase plots at period 19 in cylindrical quadrupole geometry for beam shown in Fig. 2.

The growth of transverse rms emittance for a misaligned beam exposed to image forces is shown in Fig. 4 for the round pipe and cylindrical quadrupole geometries described above. (Rms emittance is defined as $\epsilon_x \equiv (\langle x^2\rangle\langle x'^2\rangle - \langle xx'\rangle^2)^{1/2}$, and similarly for y, where $x' = dx/dz$.) The emittance in Fig. 4 is recorded once per lattice period at the center of the x focusing lens. The rms y emittance exhibits the same behavior as the x emittance, in phase with it. The beats that can be clearly seen in the cylindrical quadrupole case are not present for the round pipe case shown, though when the parameters are changed to give larger emittance growth the round pipe case also exhibits beats. The sum frequency for the beats is approximately twice the coherent betatron frequency. Note that the emittance growth for the round pipe boundary is much less than for the cylindrical quadrupoles, even though the beam has been displaced by twice as much. This is probably due to the fact that the image forces for the highly

Emittance Growth from Image Forces

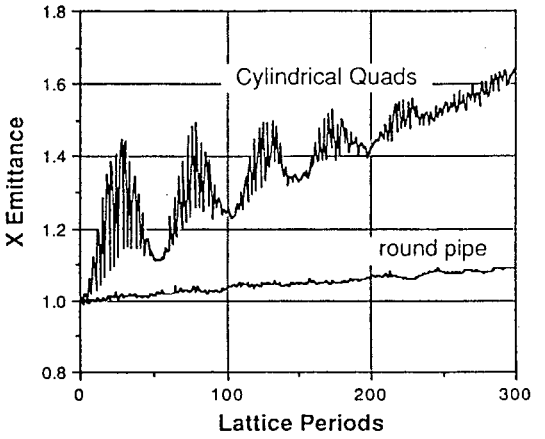

XBL 873-1323

Fig. 4. x rms emittance, normalized to its initial value, for boundary conditions described in the text. $\sigma_0 = 60°$, $\sigma = 6°$, beam major radius/distance from axis to nearest conductor = 0.42, $\theta = 45°$, h = a/4 (cyl. quads), a/2 (round pipe).

symmetric round pipe are much weaker. A few runs have been done for a Kapchinskij-Vladimirskij distribution function, which shows very similar patterns and magnitude of emittance growth.

Further characterization of the phenomenon shown in Fig. 4 can be obtained by investigating other moments of the distribution. The rms x and y radii of the beam do not vary during the run, while the rms v_x and v_y show the same behavior as the emittance. Thus, the beam is heating, not expanding. No particle loss is seen. Phase plots (see Fig. 5) show some triangularization of the beam in x-y, x-p_x, and y-p_y space, and even symmetry in x and y, indicating that the potential causing the beam deformation is odd in x and y. (Plots for the initial beam are the same as those in Fig. 5, with all axes of that figure scaled down.) This odd symmetry indicates that the distribution function will have non-zero odd multipole components, and therefore

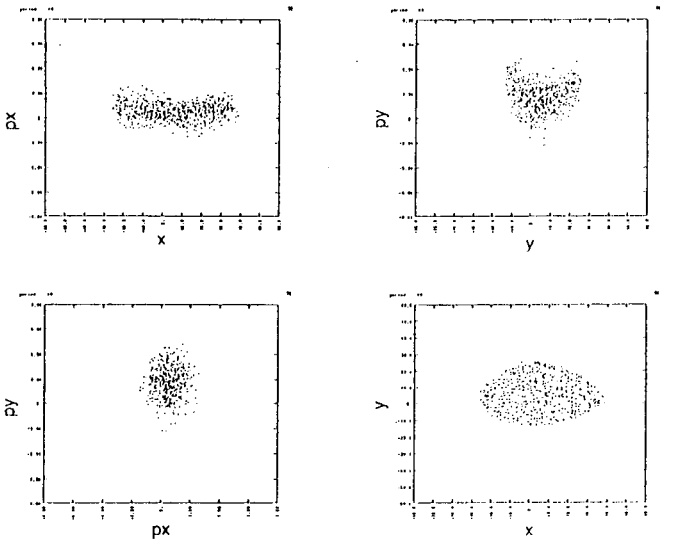

XBL 873-1321

Fig. 5. Phase plots for period 19 for cylindrical quadrupole parameters of Fig. 4.

non-zero third moments. We have therefore also looked at third order moments of the distribution function. These show beats at the same frequency as the emittance, though the sum frequency is half of that for the emittance. No secular growth of the third order moments is seen.

Thorough scaling studies have not been done, due to the extensive parameter space and the limited computer time available. The emittance growth increases with σ_0, the beam major radius, a, and the offset, h (see Fig. 1), and decreases with increasing aperture or betatron phase advance per lattice period, σ. The secular growth of the emittance is found to be approximately linearly proportional to the amplitude of the emittance oscillations.

Some experimental evidence for emittance growth due to image forces has been obtained in the Single Beam Transport Experiment,[3] in which a 120 keV Cs^+ beam is transported through 40 periods of alternating gradient focusing. Figure 6 shows the rms x emittance vs. z for two beams with different initial offset, h, from the focusing channel axis. The emittance has been calculated from the measured phase space plots using either 100% of the current or only the inner 95% in order to exclude halo effects. The emittance difference between the two beams at a given z location can be measured accurately to a few percent, but comparison at different z locations is hampered by calibration difficulties. As the graph shows, the emittance of the beam with the greater offset grows as a function of z with respect to the other beam. With h = 0 no emittance growth was seen. The magnitude of the emittance growth observed was consistent with simulation calculations, but more data would be needed to prove that the effect observed was the same as that seen in calculations.

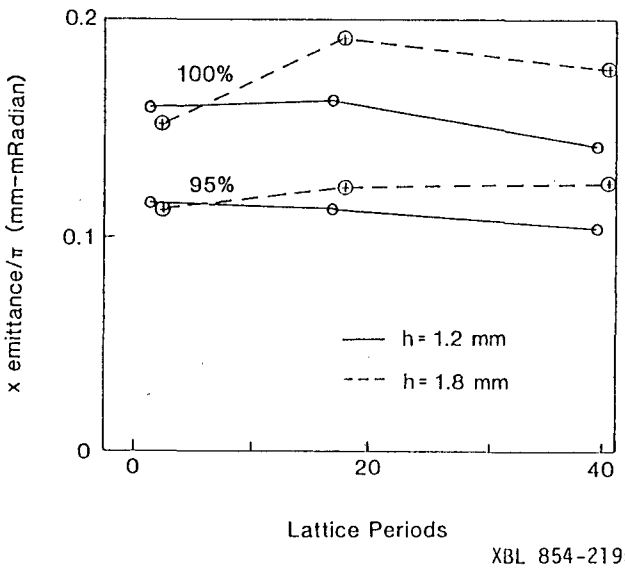

XBL 854-2195

Fig. 6. Experimental measurements of rms x emittance (circled points) for two off-center beams. $\sigma_0 = 60°$, $\sigma = 8°$.

Similar effects to those just described for image forces are seen in simulation calculations in which external nonlinear forces are present. Figure 7 shows the growth of emittance for a misaligned beam in the presence of a dodecapole potential. If quadrupole symmetry is maintained, this is the lowest order multipole which can occur as an imperfection in the focusing field. The focusing potential applied in the code is therefore $V_0[A_2(r/d)^2 \cos 2\theta + A_6(r/d)^6 \cos 6\theta]$, where d is the distance from the center of the focusing channel to the surface of the cylindrical quadrupole electrode. V_0 alternates in sign and a thin lens

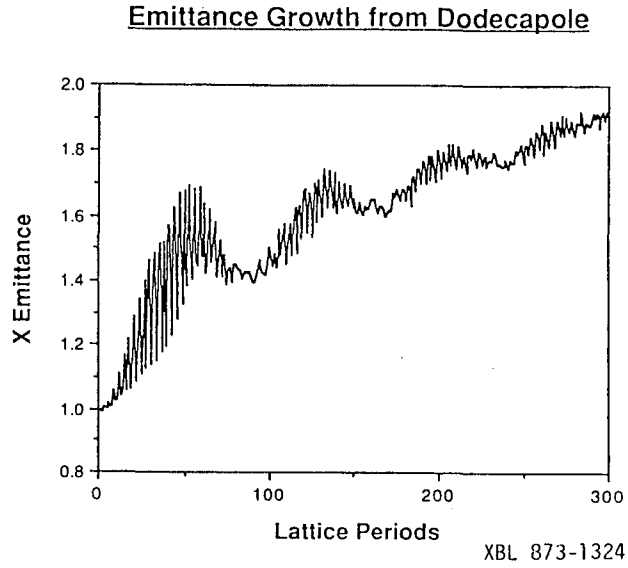

XBL 873-1324

Fig. 7. x rms emittance vs. z with external dodecapole force. $\sigma_0 = 60°$, $\sigma = 6°$, $h = a/2$, $\theta = 0°$, $A_6/A_2 = 1.02\times10^{-2}$.

approximation is used. No image forces are applied. Again, if the beam is centered in the focusing channel no emittance growth occurs. For misaligned beams a beat pattern is again seen in the emittance growth, with the sum frequency approximately equal to twice the coherent betatron frequency. The emittance growth, and also the amplitude of the emittance oscillations, appears to be proportional to A_6h, and it increases with increasing σ_0 or decreasing σ. Again the rms beam radii are essentially constant, while the rms v_x and v_y increase in the same manner as the emittance. However phase plots[5] show an odd symmetry in x and y, and therefore an even potential, indicating that while the macroscopic beam changes are similar to the image force case, the process is different in detail.

Similar effects have also been seen for an alternating sign octupole potential used to model end effects of interdigital electrostatic quadrupole structures.[5] It seems reasonable therefore to state the following as a general result: For intense space-charge-dominated ($\sigma/\sigma_0 \sim 0.1$) misaligned beams the presence of a nonlinear force causes emittance growth in a beat pattern. This is due to beam heating, with negligible change in rms beam radii.

A Possible Mechanism

The beat pattern seen in the graphs of emittance vs. z suggests that the nonlinear forces applied may be driving a coherent mode of the beam at a frequency slightly off resonance. As noted above, Hofmann et al. showed that space-charge-dominated beams in alternating gradient focusing systems have coherent modes which stabilize nonlinearly with negligible effect on beam emittance[1]. The potential of these modes is proportional to $\cos m\theta$. Figure 8 shows the phase advance per lattice period of the m = 3 or "third order" modes vs. σ for $\sigma_0 = 60°$. Note that one of the modes has a phase advance per lattice period which approaches σ_0 as the beam becomes more intense ($\sigma \to 0$). This occurs for all m. The phase advance per period of the coherent betatron oscillation is also nearly the same as σ_0, the deviation being a measure of the strength of the nonlinearity versus that of the linear focusing force. Therefore the mode frequency is close to the coherent betatron frequency. Moreover, the strength of the applied nonlinear force at the beam will be modulated at the coherent betatron frequency, since its value depends on the distance of the centroid from the axis of the focusing

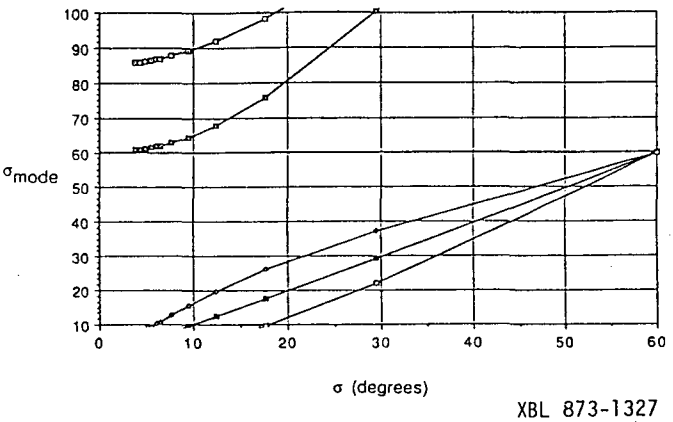

XBL 873-1327

Fig. 8. Phase advance per lattice period of the third order modes of the K-V distribution vs. σ. $\sigma_0 = 60°$.

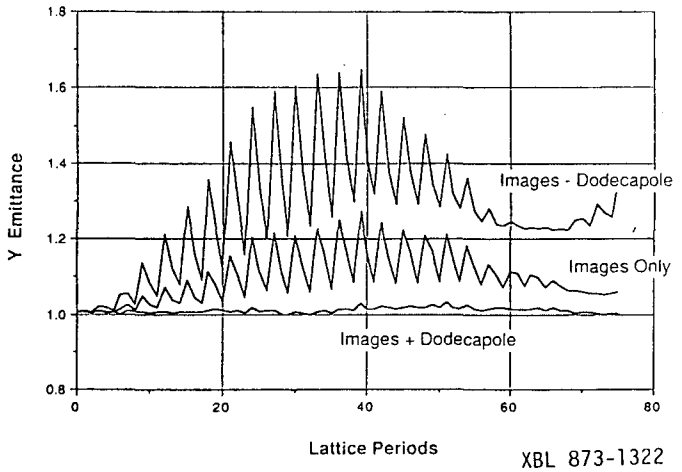

XBL 873-1322

Fig. 9. y emittance vs. z for the cylindrical quadrupole geometry and parameters of Fig. 2, with and without an additional dodecapole force, showing disappearance of emittance growth. Also shown is a case with sign of A_6 reversed. $A_6/A_2 = 1.02\times10^{-2}$.

channel. Therefore the nonlinear force provides a driving force at a frequency near the resonant frequency of these coherent modes of the beam.

The symmetry of the phase plots suggests that in the case of the image force the $m = 3$ mode might be involved, and for the dodecapole, perhaps $m = 4$. In the beam frame the image force potential does contain a $r^3 \cos 3\theta$ multipole component, and the dodecapole contains all multipoles up to 6. However we should remember that though these are the predominant symmetries evident in the phase plots, it is likely that a mixture of modes would be involved, and it is unclear that the most obvious mode in the phase plots is the one that causes the most emittance growth.

L. Smith has studied analytically the mechanism just described, for the case of constant focusing, a Kapchinskij-Vladimirskij (K-V) distribution, and the image forces in a round pipe[6]. In this case, the largest multipole component of the image forces is the third order component. Putting this into the linearized Vlasov equation with a perturbation potential proportional to $r^3 \cos 3\theta$ he found the perturbed potential to be

$$V_1 \approx \frac{\omega_0^2}{2} \frac{a^3 h^3}{R^4} \sin\left(\frac{\Omega+\omega_c}{2} t\right) \sin\left(\frac{\Omega-\omega_c}{2} t\right) \qquad (1)$$

where ω_0 is the coherent betatron frequency with no image forces or external nonlinear forces present, $\Omega = 5\omega^2 + \omega_p^2/4 + \sqrt{\omega_p^4/16 + \omega^2\omega_p^2 + 16\omega^4}$ is the frequency of a K-V third order mode being driven , with ω the betatron frequency and ω_p the plasma frequency, and R is the pipe radius. It is difficult to compare the scaling with ω_0, a, h, and R given in Eq. (1) with simulation results, since for the round pipe the emittance growth is so small. However, one can clearly see from this calculation the beat phenomenon which appears in the simulation results. The frequencies agree fairly well with the simulation calculations. This lends plausibility to the hypothesis that the emittance growth derives from the driving of coherent beam modes near their resonant frequencies by external nonlinearities or image forces, whose strength is modulated by the coherent betatron oscillation. The emittance growth itself cannot be obtained from the linearized Vlasov equation, since to this order it is zero.

Cancellation of Image Effects by the Dodecapole

When both the image forces of the cylindrical quadrupole geometry and a dodecapole force of the proper strength are present, simulation shows that the emittance growth can be reduced to zero. This is shown in Fig. 9 for the same case as Figs. 4 and 7. Though only the first 100 lattice periods are shown in Fig. 9, no emittance growth is seen over the length of the simulation run, 300 periods. This "cancellation" seems to be insensitive to the values of σ and σ_0, and is a gentle function of A_6. Since the modes driven by these two forces seem to be different, one might speculate that this "cancellation" is due to some kind of interference of one mode with the coherence of the other so that the emittance could not grow, rather than a true cancellation of the effect. However, if the sign of the dodecapole term is changed, the emittance growth is seen to double, rather than disappearing. This is shown by the third curve in Fig. 9, marked "images - dodecapole". This seems to indicate some real cancellation.

We have as yet been unable to find the mechanism by which this cancellation occurs. One reasonable hypothesis might be that both forces are driving several modes, with one primarily responsible for the emittance growth. Then if the coefficients of the multipole component of the two forces responsible for the emittance growth were made to cancel, emittance growth would not occur. The most obvious choice might be the third order mode, since it has the symmetry seen in the phase plots for the image forces. Since the image forces are present at all z in the simulation, and the dodecapole only at the lenses, they can not cancel exactly in detail. However, since we are interested in intense beams (low σ) the betatron phase advance of the particles per lattice period is low, and it is reasonable to require the cancellation of the coefficients integrated over one lattice period. We therefore find the third order multipole coefficient of both the image and dodecapole forces as seen in the beam frame (i.e., perform the multipole expansion about the beam centroid), average them over one lattice period, and set the coefficients for the two forces equal and opposite. This has been done analytically, using the image force due to four hyperbolic electrodes rather than the cylindrical ones used in the simulation. The result gives a value of A_6 for cancellation which is a factor of 10 higher than the value which the simulation shows to cause cancellation. Moreover, using in the simulation the value of A_6 calculated analytically causes extreme emittance growth. If we attempt to follow the same procedure, but assume that the mode of interest is the fifth order mode, then we again find disagreement with the simulation, the value of A_6 calculated analytically being a factor of 4 less than the simulation value. So at this

time we can only say that the mechanism of cancellation is not understood. It may be that it is not necessary to completely cancel the driving force in order to stop emittance growth, but only to bring it below some threshold for growth--we know, for instance, that nonlinear stabilization of the modes occurs when they are started with a small perturbation and no driving force is present. This could account for the fact that the analysis finds a larger third order dodecapole component necessary for cancellation than the simulation shows is needed. Another possibility is that the mechanism is nonlinear and does not involve straightforward cancellation of the driving forces.

We have been unable to produce similar cancellation to that of the cylindrical quadrupole case in the simulation results for the round pipe image force by any simple scaling of input parameters or analytical calculations. However no systematic variation of the parameters to find a minimum of the emittance growth has yet been done.

Summary and Conclusions

We have shown using particle-in-cell simulation that in an alternating gradient focusing system in the presence of (1) image forces due to either of two different conducting boundary geometries, or (2) dodecapole or octupole imperfections of the focusing fields, transverse emittance growth occurs for misaligned intense ($\sigma/\sigma_0 \sim 0.1$) beams. This appears to be a general phenomenon caused by the driving of stable coherent modes of the beam by the nonlinearity, and we expect that it will occur for other nonlinear forces besides those mentioned above. The frequency of modulation of the nonlinearity strength, the coherent betatron frequency, is nearly coincident with the frequency of some coherent modes for intense beams, enabling the nonlinear force to drive these modes near their resonant frequencies.

For the case of the image forces of cylindrical quadrupole electrodes simulation has shown that emittance growth can be prevented by applying a dodecapole force of the correct strength. Analytical theory shows that this is not due to a straightforward cancellation of the driving force of the most likely modes, and the mechanism for the effect is not yet understood.

Analysis of data from the Single Beam Transport Experiment indicates a growth of rms emittance for misaligned beams, but further experiments are needed to assess the validity of both the growth of emittance and the image-dodecapole cancellation seen in simulation results.

The practical consequences of the effects we have discussed depend on the amount of emittance growth that is tolerable in a given experiment, the length of the accelerator, and the diameter of the beam. The beam diameter is important since it gives the scale length for acceptable misalignments, and technological limits on this length of course exist. In general, for a given allowable emittance growth the phenomena described will specify limits on the amount of misalignment which is permissible, given the strength of the nonlinear forces acting and the value of σ/σ_0. From another point of view, given the technologically achievable alignment of a beam and the lower limit on spurious focusing field nonlinearities, the effects described give a lower limit on the value of σ/σ_0 which can be transported without exceeding limits on emittance growth for a given length accelerator. For Heavy Ion Fusion this does not place unacceptably low limits on the alignment of the beam or the charge per unit length that can be transported. Results like those shown in Fig. 4 indicate that emittance growth due to the image forces of a round pipe is small enough to be tolerable in the ~ 400 periods needed for a reactor, assuming reasonable misalignments of $h \leq a/4$.

References

[1] H. Hofmann, L.J. Laslett, L. Smith, and I. Haber, Particle Accel. 13, p. 145 (1983).

[2] I. Haber, AIP Conference Proc., No. 152, Proc. 1986 International Symposium on Heavy Ion Fusion (Washington, D.C., 1986), p. 236 (1986).

[3] M.G. Tiefenback and D. Keefe, Trans. on Nuc. Sci. NS-32, p. 2483 (1985).

[4] I. Haber, Proc. 1984 INS International Symposium on Heavy Ion Accelerators and Their Applications to Inertial Fusion, p. 451 (Institute for Nuclear Study, Tokyo; 1984).

[5] C.M. Celata, V.O. Brady, L.J. Laslett, and L. Smith, IEEE Trans. on Nuc. Sci. NS-32, p. 3193 (1985).

[6] C.M. Celata, I. Haber, L.J. Laslett, L. Smith, and M.G. Tiefenback, IEEE Trans. on Nuc. Sci. NS-32, p. 2480 (1985).

Acknowledgments

The author would like to acknowledge the contributions of several people to the work presented in this paper. Foremost are the contributions of Lloyd Smith, who suggested the problem initially, derived many of the analytical results presented, and guided the project throughout. We also gratefully acknowledge many helpful discussions with L. Jackson Laslett, as well as his work on hyperbolic electrode images and his results as presented in Fig. 8. The simulation code was written by Irving Haber of Naval Research Laboratory, who gave consistently helpful advice on the numerical aspects of the problem. Michael Tiefenback produced the experimental results quoted, and we are grateful to him also for useful discussions about the experiment.

SPACE CHARGE EFFECTS IN A BENDING MAGNET SYSTEM*

E.P. Lee, E. Close and L. Smith
Lawrence Berkeley Laboratory
University of California
Berkeley, CA 94720

Abstract

In order to examine problems and phenomena associated with space charge in a beam bending system, the beam dynamics code HICURB has been written. Its principal features include momentum variations, vertical and horizontal envelope dynamics coupled to the off-axis centroid, curvature effect on fields, and images. Preliminary results for an achromatic lattice configuration are presented.

Introduction

The transport of intense ion beams in strong focussing lattices has been the subject of theory and experiment for eleven years.[1-4] However, the consideration of such beams in a system which includes bends has only recently begun. In particular, this report is concerned with the bending of an intense beam bunch of finite length, in which the momentum varies from head to tail of the bunch.

In an intense ion beam, space-charge induced forces play a role comparable to or greater than emittance in determining the envelope radii. A quantitative measure of intensity is the degree of tune depression by the beam's space charge. If (σ_0) denotes the undepressed tune (phase advance per lattice period), then the depressed value (σ) experienced by an ion is approximately given by

$$\sigma^2 \simeq \sigma_0^2 - K\left(\frac{2L}{\bar{a}}\right)^2 .$$

Here $\bar{a}$ is the mean beam edge radius, L is the lattice half period length, and K is the perveance,

$$K = \frac{2qeI}{(\beta\gamma)^3 Mc^3 4\pi\epsilon_0} ,$$

where I is ion current, q and M are charge state and mass, and $\beta\gamma$ is the relativistic factor. Space charge forces dominate over emittance when $\sigma/\sigma_0 \leq 1/\sqrt{2}$. It has been demonstrated[5] that transport is stable over many lattice periods (≥ 40) provided that $\sigma_0 < 85°$ and $\sigma/\sigma_0 \gtrsim 0.1$. For a short transport subsystem consisting of only 10-20 lattice periods, such as might be employed with an inserted bend of, say, 180°, it is expected (but has not been demonstrated) that these conditions could be relaxed to $\sigma_0 \leq 90°$, $\sigma \geq 0°$.

The introduction of bends raises the issue of the control of chromatic effects. For a low current beam there are many combinations of bends and quadrupoles which result in a first order, double achromat, i.e., the first order optics of the complete subsystem is independent of small differences of momentum ($\Delta P/P$) among ions. This is generally desirable for a single bend followed by a straight system since any dependence of final transverse phase space variables on ΔP would convert momentum spread into an effective increase in emittance. Similarly, a momentum variation along a pulse (without local spread) would result in an undesirable time dependent jitter in position and angle of the beam centroid.

*This work was supported by the USASDC under Contract No. MIPR W31RPD-63-A087 and also by the Office of Energy Research, Office of Basic Energy Sciences, U.S. Department of Energy, under Contract NO. DE-AC03-76SF00098.

For an intense ion beam, special care must be taken in the design of an achromat since the focussing and bending forces are modified by beam-induced fields. In particular, any portion of a beam pulse with mean momentum deviation ΔP is displaced from the design orbit by the local centroid value $X = (\Delta P/P)d$ where d is the dispersion. This displacement induces an image force directed towards the conducting boundary of approximate magnitude XK/R^2 where R is the pipe radius.

The image force acts in first order as a defocussing element in the centroid dynamics. Ideally the focal strength of the lattice should be increased to compensate for the image effect in order to restore the desired achromatic condition. This is impossible to do in general since the current varies along the pulse. It is also clear that the dispersion function of the centroid differs from that of an individual particle since the particles are subject to the full tune depression of the beam's self field, while the centroid is subject to the (smaller) image force. For the present study we consider the situation in which momentum spread is negligible at any position within the beam pulse, but varies by a large amount (up to 8% total) along the pulse. The centroid dynamics are of the greatest concern and we seek a bending configuration which does not cause unacceptable jitter of the centroid.

To aid in this study a beam dynamics code HICURB has been written. In its preliminary version it contains a treatment of the beam envelope and centroid in a system of bends and quadrupoles, including the image forces. A future version of HICURB will also incorporate the modification of beam-induced fields resulting from curved geometry, which affects centroid dynamics in the same order of approximation as the image force.

Bend System

The specific computations described here were carried out for a bend system composed of eight periods, all of the identical form FOBODDOBOF, for a total of eighty lattice elements. If the total angle of bend is 180° then each of the sixteen bend magnets, (B), deflects the beam through some 11.25°. Adjacent elements of the same type would be combined in the physical lattice. Focus (F) and defocus (D) quadrupoles are of equal strength and produce an undepressed tune $\sigma_0 = 90°$. Individual quadrupoles, bends (B) and drifts (O) occupy respectively 1/12, 1/6, and 1/12 of the lattice space and are treated in hard edge approximation. Curvature and edge focussing are neglected in the present version of HICURB. The cumulative bend is 180° with total length (16L). A double achromatic condition ($d = d' = 0$) occurs at the system midpoint and end in the absence of beam induced fields. This feature is a consequence of the symmetric placement of elements and the 720° total phase advance. Achromats of this general type may be made up out of sectors with 360° phase advance, each sector containing $n \geq 3$ identical periods with $\sigma_0 = 360°/n$. The larger values of n yield weaker focussing for a fixed period length (2L), but have smoother envelopes and are possibly less prone to intense-beam instabilities. The use of two 360° sectors with $\sigma_0 = 90°$ is a natural choice for a bending system using a minimum of space and characterized by large momentum variations (±4% from the center of the bunch) because of its tight focus using magnets of reasonable length and aperture. The maximum beta function and dispersion in the absence of space charge are

$$\beta_{max} = (3.2763)\ L\ , \qquad d_{max} = (1.0511)\ L\ .$$

The quadrupole field gradient (for $\sigma_0 = 90°$) is

$$B' = (4.8164)[B\rho]/L^2\ ,$$

where $[B\rho] = \beta\gamma Mc/qe$ is the magnetic rigidity of the ions.

Image Field

The image field of a beam of elliptic cross section, centered off-axis in a circular cross section pipe is employed in HICURB. We note first that it is sufficient to obtain an expression for the electrostatic field alone since in straight-pipe geometry, the transverse force from magnetic field is incorporated by the substitution

$$\underset{\sim}{E} + \underset{\sim}{v} \times \underset{\sim}{B} \rightarrow \underset{\sim}{E}/\gamma^2\ .$$

The Greens function solution for the image field is

$$\underset{\sim}{E}(\underset{\sim}{r}) = -\frac{1}{2\pi\epsilon_0}\underset{\sim}{\nabla}\int d^2r'\rho(\underset{\sim}{r'})\ \log\left|\frac{R^2\underset{\sim}{r'}}{r'^2} - \underset{\sim}{r}\right|\ ,$$

where $\rho(\underset{\sim}{r'})$ is the charge density of the beam and R is the pipe radius. A convenient expression for the field is

$$E_x + iE_y = \frac{1}{2\pi\epsilon_0 R^2}\int d^2r'\ \frac{\rho(\underset{\sim}{r'})(x'+iy')}{1 - (x'+iy')(x-iy)/R^2}\ .$$

From this form we obtain the expansion in inverse powers of R^2:

$$E_x + iE_y = \frac{\lambda}{2\pi\epsilon_0 R^2}\left[\overline{(x+iy)} + \frac{\overline{(x+iy)^2}\ (x-iy)}{R^2} + \frac{\overline{(x+iy)^3}\ (x-iy)^2}{R^4} + \ldots\right]\ .$$

Performing the averages over an ellipse of semi-axes (a,b), and displaced by amount $X \equiv \bar{x}$, we have, through order X^3

$$E_x + iE_y = \frac{\lambda}{2\pi\epsilon_0 R^2}\left[(x-X)f - iyf + Xg\right]\ ,$$

where f and g are defined as

$$f = \frac{a^2-b^2}{4R^2} + \frac{X^2}{R^2}\left[1 + \frac{3}{2}\left(\frac{a^2-b^2}{R^2}\right) + \frac{3}{8}\left(\frac{a^2-b^2}{R^2}\right)^2\right]\ ,$$

$$g = 1 + \frac{a^2-b^2}{4R^2} + \frac{X^2}{R^2}\left[1 + \frac{3}{4}\left(\frac{a^2-b^2}{R^2}\right) + \frac{1}{8}\left(\frac{a^2-b^2}{R^2}\right)^2\right]\ .$$

The leading term $(\lambda X/2\pi\epsilon_0 R^2)$ is the usual dipole force induced by small displacements of a beam with circular cross section. There are also a quadrupole force term induced by the elliptic cross section and terms of order X^2 and X^3 which couple the centroid to the envelope oscillations.

Code Model

In its preliminary form HICURB solves the coupled envelope equations of Kapchinskij and Vladimirskij[5] with the additional quadrupole force terms resulting from the image field:

$$\frac{d^2a}{ds^2} = \pm\frac{B'}{[B\rho]}a + \frac{\epsilon_x^2}{a^3} + \frac{2K}{a+b} + \frac{Kaf}{R^2}\ ,$$

$$\frac{d^2b}{ds^2} = \mp\frac{B'}{[B\rho]}b + \frac{\epsilon_y^2}{b^3} + \frac{2K}{a+b} - \frac{Kbf}{R^2}\ .$$

The function f contains the effects of the round pipe image resulting from the non-zero centroid X and elliptic profile of the beam.

The centroid in the bend plane $[X(s)]$ is the mean value of particle amplitude x. An equation of motion for X is obtained by taking an average over the single particle equation, assuming the particles uniformly occupy a displaced ellipse of semi-axes a and b. We find

$$\frac{d^2X}{ds^2} = \pm\frac{B'}{[B\rho]}X + \frac{\Delta P}{P}\frac{1}{\rho} + \frac{KXg}{R^2}\ ,$$

where ρ is the radius of curvature in the bends and g is the previously defined image function.

In a periodic lattice there exist matched periodic solutions for the envelope radii and X. The initial values for these matched solutions in the absence of images are available in tabular form or may be found directly by solving of the model equations, omitting images.

It is clear that the code model is incomplete at this stage and the computed results should in any event serve only as a guide to the magnitude of disturbance by images and its possible compensation. A particle-in-cell simulation should be used in conjunction with HICURB to provide greater detail and physical insight. Model features which we intend to add to HICURB are

a. Modification of fields due to curved geometry

b. Energy variation with time resulting from motion in an electrostatic potential

c. Curvature and edge focussing from bends

d. Non-circular pipe boundary

e. Time variation of perveance due to bunching.

Code Description

The numerical results presented in this report were obtained using a preliminary version of the FORTRAN-77 program HICURB, which was written at LBL during 1986. This program consists of the main program, HICURB, and a collection of modules that perform the necessary programming and calculation tasks such as lattice element definition and arrangement and input/output features.

Lattice elements are described in terms of their geometric length and aperture, along with magnetic field properties appropriate for their type. The system is defined using a simple list representation that allows sections of the system to be defined and subsequently used in repetitive or reflected blocks. This allows a system of many elements to be easily represented once the elements in a half-period are specified. The input beam parameters are the ion charge state, mass number, kinetic energy, current, momentum error, and horizontal and vertical emittances. Perveance, magnetic rigidity and radius of curvature are then computed.

A standard fourth-order Runge-Kutta integration package is used to integrate the six first-order equations for

beam radii, centroid displacement, and their derivatives. A hard-edge magnet representation was used to obtain the results of this report. However, HICURB is capable of performing calculations with any variation of field. Integration parameters have been set to give 6 or 7 significant figures. The calculation for the particular system considered in this study, consisting of 80 elements, is easily performed on a VAX/VMS 8600 system in a few seconds of CPU processing time.

HICURB will be modified as experience is acquired and new model features are developed. Because of the program's modular construction it is easy to introduce system editing modules, specific diagnostic output, and graphical output. It is also easy to change the program to reflect the changes in the model. Because HICURB is actually a generic program for defining systems and calculating systems element by element, it is not difficult to include features such as ray tracing or element transformations.

Computation Study

HICURB has been used in its preliminary form to study the effect of images on the beam envelope and centroid. The above described lattice is used, with input parameters.

$$K = 7.0827\times10^{-4}, \qquad L = 5.8905\times10^{-1}\ \text{m}$$

$$\epsilon_x = \epsilon_y = 0, \qquad \rho = 1\ \text{m}\ .$$

In order to study intense beam phenomena, the tune has been depressed to zero ($\sigma = 0$) with matched initial radii (ignoring image forces):

$$a(0) = a_{max} = \left(2.9952\times10^{-2}\ \text{m}\right)$$

$$b(0) = a_{min} = \left(1.4988\times10^{-2}\ \text{m}\right),$$

and $a'(0) = b'(0) = 0$. The matched initial value of X is

$$X(0) = X_o = \left(1.2383\times10^{-2}\ \text{m}\right)\left(\frac{\Delta P/P}{.04}\right),$$

$$X'(0) = 0\ .$$

An initial run with $R = \infty$ was made to verify the matched solutions undisturbed by images, and obtain the maximum, matched, undisturbed derivatives ($a'_{max} = 3.68717\times10^{-2}$, $X'_{max} = 1.65012\times10^{-2}$), which provide a basis for comparison with the disturbed solutions.

Three pair of runs were made to compare the envelope and centroid values obtained using pipe radii $R = .12$ m and .06 m with the undisturbed values. The final values, taken at the system end, are of greatest importance since they give an indication of the violation of achromaticity.

The first set of runs takes $\Delta P/P = 0$, so $X = 0$ everywhere and the only image effect is the small additional quadrupole force from the elliptic profile [$= (Ka/R^2)(a^2-b^2)/4R^2$]. Denoting final values by subscript f we find

$$\left.\begin{aligned} a_f/a_o &= 1.00002 \\ a'_f/a'_{max} &= -3.87\times10^{-5} \end{aligned}\right\} R = .12\ \text{m}\ ,$$

$$\left.\begin{aligned} a_f/a_o &= 1.00036 \\ a'_f/a'_{max} &= -5.980\times10^{-4} \end{aligned}\right\} R = .06\ \text{m}\ .$$

Hence there are very small decreases in the effective value of σ_o, with inconsequential results.

The second set of runs takes $\Delta P/P = .04$ corresponding to the bunch tail, and $X(0) = X'_o(0) = 0$, i.e. the centroid is not matched. In the absence of images, a, a', X and X' return to their initial values at the system end. However, we obtain with images

$$\left.\begin{aligned} a_f/a_o &= .99941 \\ a'_f/a'_{max} &= -1.0737\times10^{-3} \\ X_f/X_o &= 3.0715\times10^{-2} \\ X'_f/X'_{max} &= -9.6663\times10^{-2} \end{aligned}\right\} R = .12\ \text{m}\ ,$$

$$\left.\begin{aligned} a_f/a_o &= 1.0319 \\ a'_f/a'_{max} &= -2.3074\times10^{-2} \\ X_f/X_o &= 7.0203\times10^{-1} \\ X'_f/X'_{max} &= -3.9529\times10^{-1} \end{aligned}\right\} R = .06\ \text{m}\ .$$

A very considerable (and probably unacceptable) disturbance of the centroid has developed for the case $R = .06$ m. With $R = .12$ m there is an improvement factor of several for X_f and X'_f.

The third run set takes $\Delta P/P = .04$ (the bunch tail) and matches the centroid [$X(0) = X_o$, $X'(0) = 0$]. This yields

$$\left.\begin{aligned} a_f/a_o &= 1.00004 \\ a'_f/a'_{max} &= -2.57\times10^{-5} \\ X_f/X_o &= 1.00105 \\ X'_f/X'_{max} &= -3.3049\times10^{-3} \end{aligned}\right\} R = .12\ \text{m}\ ,$$

$$\left.\begin{aligned} a_f/a_o &= 1.00427 \\ a'_f/a'_{max} &= -3.1334\times10^{-3} \\ X_f/X_o &= 1.0944 \\ X'_f/X'_{max} &= -5.5898\times10^{-2} \end{aligned}\right\} R = .06\ \text{m}\ .$$

The final values obtained with $R = .12$ m and possibly $R = .06$ m may be acceptable for most laboratory applications. However, it may prove difficult to obtain the matched initial conditions without introducing an image disturbance in the matching sections.

The authors would like to thank L.J. Laslett for a useful table of matched envelope parameters and D. Keefe and T. Fessenden for useful advice on system definition.

References

[1] E.D. Courant, ERDA Summer Study of Heavy Ions for Inertial Fusion, LBL-5543, 72, (1976) [An account of A. Maschke's work is given].

[2] I. Hofmann, L.J. Laslett, L. Smith, I. Haber, Particle Accelerators, 13, pp. 145, (1983).

[3] C.M. Celata, I. Haber, L.J. Laslett, L. Smith, M.G. Tiefenback, "The Effect of Focusing Field Nonlinearities in MBE-4 on Transverse Beam Dynamics," IEEE Trans. Nuc. Sci., NS-32, No. 5, pp. 2480-2482 (1985).

[4] M. Tiefenback, D. Keefe, IEEE Trans. Nuc. Sci., NS-32, No. 5, pp. 2483, (1985).

[5] I.M. Kapchinskij and V.V. Vladimirskij, Proc. Int. Conf. on High Energy Accelerators, CERN, pp. 274, (1959).

TRANSVERSE COMBINING OF NONRELATIVISTIC BEAMS IN A MULTIPLE BEAM INDUCTION LINAC*

C.M. Celata, A. Faltens, David L. Judd, L. Smith, and M.G. Tiefenback†
Lawrence Berkeley Laboratory
University of California
Berkeley, CA 94720

Abstract

Emittance growth of beams during transverse combining has been studied computationally and experimentally for Heavy Ion Fusion applications, and the theory and results are presented. A hardware design is also discussed.

1. Motivation

At the low energy end of an inertial confinement fusion heavy ion driver it is most cost effective to transport the intense beams by dividing the current into many "beamlets" which are individually focused by an array of magnetic or electrostatic focusing quadrupoles. The desirability of dividing the current into many beams is a result of the fact that if the aperture radius of the quadrupoles is decreased while keeping the highest technologically possible field at the pole tip, a higher focusing field gradient results, making possible the transport of a higher current density beam. The advantage gained by going to smaller aperture must be weighed against two factors. First, as the beam radius decreases, the clearance needed for misalignments and mismatches increases slowly. Thus little gain is made in decreasing the aperture by decreasing the charge per unit length when the beam radius becomes smaller than the required clearance length. Second, the increased number of focusing elements required to transport the larger number of beams increases the cost of the focusing system. For a heavy ion inertial confinement driver, minimal cost occurs when the number of beams at the low energy end is about 100. At the high energy end of the accelerator, where space charge forces are weaker relative to available focusing, the optimum number of beamlets is approximately 8-16. Therefore it is necessary at some point to combine beams, probably in the 100-500 MeV range.

In this paper we will consider transverse combining of intense beams. Beam combining is permitted only if the resultant emittance growth is tolerable. Considering target requirements and the best available sources, a total emittance increase of about 100 times is allowed in the accelerator.

2. A Combining System

To date, we have considered only the four-to-one combining of beams because of the relevance of this arrangement to the square arrays of multiple beams presently envisioned for future experiments. The combining section will deflect the centroids of the beams through a bend, followed by a reverse bend, so that when they emerge into a common focusing channel their centroids are as close together as possible, with negligible relative transverse velocity. Both of these constraints are needed to minimize the emittance growth when the beams combine.

During the bending process, it may be advisable to maintain individual A-G focusing of the beams. Making the reasonable assumption that the strength of the bending fields will be limited to values of the order of the limit on the focusing field strength, it can be shown that without concurrent focusing the beam radii will double in the bends. This may make an array of such beams unacceptably large. A sketch of a possible combining section is shown in Fig. 1.

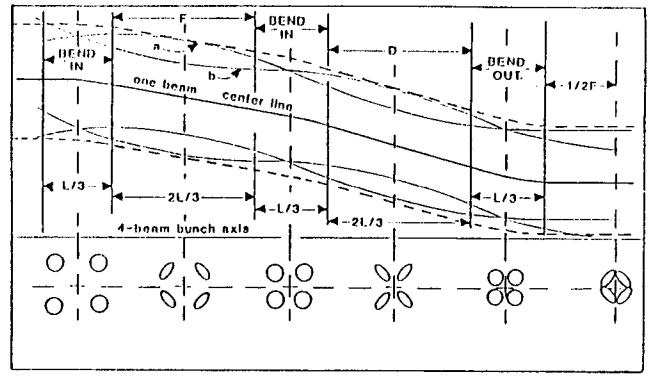

XBL 8611-4313

Fig. 1. Above are shown successive bending and focusing regions and x and y envelopes a and b, for one of the four beams. Also indicated are the transverse sections of all four beams at the six stations shown.

In order to bring the beams as close together as possible, the structure between them which provides the focusing and bending fields at the end of the bending section must be thin. It appears possible to use pulsed current-sheet magnetic dipole and quadrupole field arrays for this purpose. Because the fields are only needed for microseconds and the duty cycle is low, conducting sheets as thin as a few millimeters can be used. A set of four dipole fields needed to bring the four beams together can be realized by various current-sheet configurations. Quadrupole fields can be generated by various configurations of current sheets having a linear variation of current density across them, but they require an outer layer of permeable material to guide magnetic flux around the outside of the arrays. All of the required current distributions can be made to adequate accuracy by relatively small numbers of conducting wires, rather than continuous sheets.

3. Emittance Growth

Emittance growth due to the combining process occurs for two reasons. First, the betatron orbits of the particles cause them to fill in "holes" between the beams in phase space which are present when they first emerge into the same focusing channel, causing what we will call "geometric" emittance dilution. This is well known, and has been studied in the context of stacking in storage rings. Second, space charge forces cause the density profile to change, rapidly expanding the beams into the spaces between them in configuration space. The change in electrostatic field energy becomes transverse kinetic energy.

In this paper we will be interested in the change in the transverse rms emittance, defined as $\epsilon_x \equiv (\langle x^2\rangle\langle x'^2\rangle - \langle xx'\rangle^2)^{1/2}$, and similarly for y. We will assume that the initial configuration of beams as they emerge from the combining section described above is "rms matched" to the focusing lattice -- i.e., that the rms beam radii of the total configuration are the same as those of a uniform matched beam. This implies that in general the x and y emittances of the configuration are not equal. Further, we assume that since the composite beam is "rms

*This work was supported by the Office of Energy Research, Office of Basic Energy Sciences, U.S. Dept. of Energy under Contract No. DE-AC03-76SF00098.

†Present address: Pulse Sciences, San Leandro, CA.

matched" to the focusing channel, the rms radii of the final combined beam are these same matched radii. Simulation shows this to be a reasonable assumption if the beams are very close together -- within a few beam radii of each other. In this case the geometric emittance dilution can be easily calculated from the initial conditions. Experiments on a single beam in the Single Beam Transport Experiment at Lawrence Berkeley Laboratory have shown that space charge couples the transverse dimensions, causing the final beam to have equal emittance in the two planes. We therefore assume the final x and y emittances to be equal. Finally, if the configuration of beams is matched, then the sum of the electrostatic field energy and the transverse kinetic energy, measured at homologous points in the focusing lattice, will be constant. Using this we obtain:

$$\frac{\epsilon_{fx}}{\epsilon_{ox}} = \sqrt{\frac{\langle x^2\rangle\, \epsilon_{oy}/\epsilon_{ox} + \langle y^2\rangle - \langle y^2\rangle\, \Delta U/T_{ox}}{\langle x^2\rangle + \langle y^2\rangle}} \qquad (1)$$

and similarly for y , where ΔU is the change in electrostatic field energy per unit length (note that $\Delta U < 0$), T_{ox} is $Nmv_{xo}^2/2$, N is the number of particles per unit length, and "o" and "f" refer to the initial state of the configuration of four beams emerging from the bending section and the final state respectively.

ΔU can be calculated if the final density profile of the beam is known. Strückmeier et al.[1] have indicated that, based on simulation, the equilibrium state of a space-charge-dominated beam in a linear focusing system seems to have a uniform density profile. Hofmann and Strückmeier[2] have shown that this is the profile which has the lowest electrostatic field energy. We therefore assume the final beam to have uniform density. We have studied in some detail the configuration of beams shown in Fig. 2. We will discuss the results below, and then comment briefly on the case shown in Fig. 1, where two of the beams have their major axes rotated by 90 degrees.

ΔU can be found analytically for the geometry of Fig. 2 for the case of constant focusing and round beams, with $\delta_x = \delta_y$. Assuming a final state of uniform density, with initial and final rms radii equal,

$$\Delta U = \frac{N^2q^2}{64\,\pi\epsilon_0}\left\{3-4\ln\left[\frac{1-g^8}{4}\left(\frac{a}{\delta}\right)^3\left(1+2\,\frac{\delta^2}{a^2}\right)^2\right]\right. \qquad (2)$$

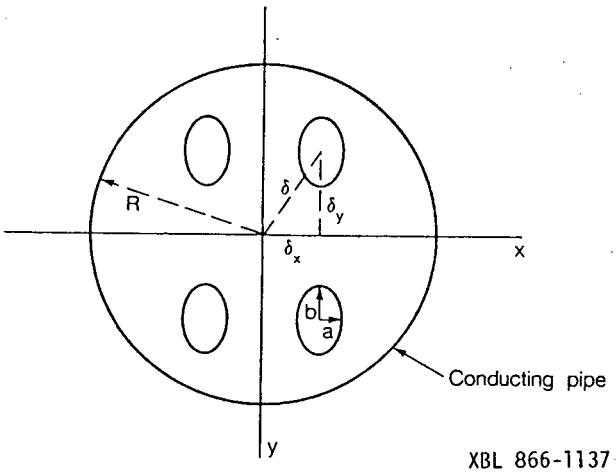

Fig. 2. Transverse plane geometry showing four beams when they first "see" each other. The separation of the beams is exaggerated in this diagram.

where q = charge of the ion, $g = \delta/R$, a is the beam radius, and δ is defined in Fig. 2. Note that there is negligible dependence on g, so that ΔU depends only on δ/a and Nq. For all configurations of beams U, and therefore ΔU, will be proportional to N^2q^2, and this is the only explicit dependence of the total emittance dilution on Nq. Using Eq. (1) the emittance growth due to space charge alone can now be shown to be

$$\Delta(\epsilon^2) \equiv \epsilon_{fx}^2 - \epsilon_{ox}^2 = -\frac{1}{Nmv_z^2}\langle x^2\rangle\,\Delta U = -\frac{q^2}{32\,\pi\epsilon_0}\,\frac{\Delta U}{kE^2} \qquad (3)$$

where k is the focusing constant and $E = mv_z^2/2$. Equation (3) was used to calculate the results of varying the beam charge per unit length while keeping constant σ_0 and the value of $c = 2^{-1/2}\,\delta - a$. c is defined as the clearance between a beam and the x (or y) axis, and therefore the clearance to the conducting sheets separating them before they combine. As Nq increases, "a" will increase as $(Nq)^{1/2}$. For the experimentally interesting range of σ_0 = 30°-80°, c = 3-6 mm, and Nq = .01-0.2 μC/m, the variation of $\sqrt{\Delta(\epsilon^2)}$ with Nq was found to be very close to linear. This is not true for smaller values of Nq. As expected, $\Delta(\epsilon^2)$ increases with c.

The total emittance growth can be defined as $M_x = (\epsilon_{ox}/(2\epsilon_{ix})(\epsilon_{fx}/\epsilon_{ox})$, where the first factor is the geometric emittance dilution, the second we will refer to as the space charge factor, and ϵ_i is the emittance of one beamlet before combining. Note that if phase space were exactly conserved during combining, the value of M would be unity. For the round beam case the geometric factor is $0.5\sqrt{1+2\delta^2/a^2}$. The total emittance growth is seen from Fig. 3 to be about a factor of four for experimentally feasible parameters.

The combining geometry of Fig. 2 was also investigated for the case of elliptical beams in a A-G focusing system, using the 2D particle-in-cell simulation SHIFTXY. The initial particle distribution for each beam was assumed to be gaussian in velocity, with uniform temperature, and uniform in density. The betatron phase advance per lattice period, σ, and the emittance of the beamlets before combining, as well as σ_0, R, and the rms radii of the initial configuration, were kept constant for all runs. When $\zeta = 1$, where $\zeta \equiv (\delta_x/a)/(\delta_y/b)$, simulation results for the emittance growth had the values which would be calculated using the value of ΔU given for round beams, with $\delta = \sqrt{2}\,\delta_x$. The results are therefore parameterized in terms of the values of this shape factor, ζ, which

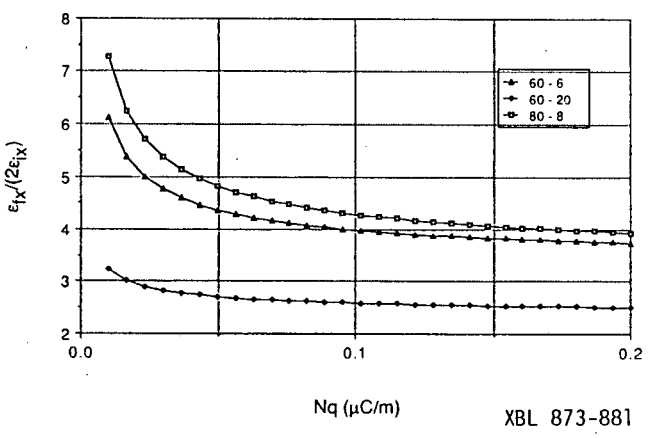

Fig. 3. Emittance increase during combining for a = b, $\delta_x = \delta_y$, calculated from Eqs. (2),(3). c = 3 mm, L = 0.5 m. The legend identifies the betatron phase advance per meter with and without space charge for each curve.

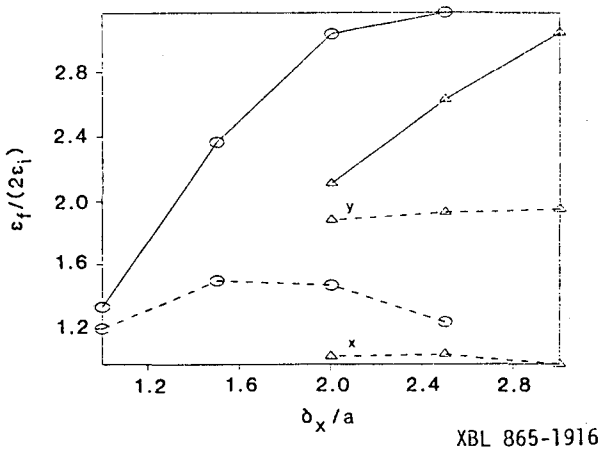

Fig. 4. One dimensional rms emittance growth vs. δ_x/a for $\zeta = 1$ and $\zeta = 2$. Circles and triangles are simulation results for $\zeta = 1$ and $\zeta = 2$ respectively. Solid lines are total emittance growth, $\epsilon_{fx}/(2\delta_{ix})$, while dashed lines are space charge dilution factor only. $\sigma_0 = 60°$, $\sigma = 20°$ (before combining), x_{rms}/R for initial configuration = 0.35.

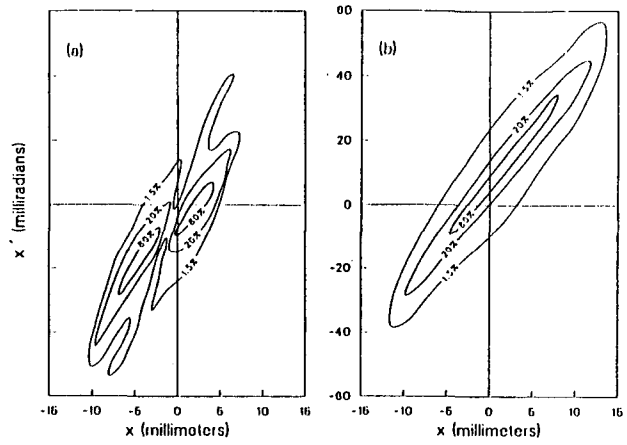

Fig. 5. Phase plots for the last case in Table 1. x vs. x' measured for (a) 0.5 and (b) 38.5 lattice periods downstream of the mask. Total current after the mask = 4.2 mA.

indicates the departure from "roundness", and δ_x/a. With the value of $\langle x^2\rangle/\langle y^2\rangle$, these two parameters specify the initial state. The results are shown in Fig. 4. As δ_x/a increases, keeping $\langle x^2\rangle$ constant, "a" must decrease, giving hotter initial beams, since the emittance per beam is constant. In an actual experiment, this would be done using a matching section. The additional energy provided by the combining then gives a smaller fractional increase in the transverse kinetic energy, and therefore in the emittance. This effect accounts for the fact that the space charge emittance factor seen in Fig. 4 does not rise monotonically with δ_x/a but instead attains rather moderate values and then levels off or decreases. Note that for experimentally realizable parameters the values of emittance growth are less than or equal to a factor of about 3. As explained above, these results imply that beams may be combined a few times in a heavy ion inertial fusion linac driver without causing unacceptable emittance growth. A few simulation runs have been done for the case of beams in the configuration shown in Fig. 1. These show emittance growth of the same magnitude as the cases just described, with values of M_x, M_y less than or equal to about 3.

The Lawrence Berkeley Laboratory Single Beam Transport Experiment[3] was used to test the theoretical results for emittance growth described above, by intercepting the space-charge-dominated 122 keV, 10 ma, Cs^+ beam with a conducting plate with four holes cut in it, in the geometry shown in Fig. 2. The normalized rms beam emittance upstream of the mask was $0.26\times10^{-7}\,\pi$ m-rad. The plate was placed at a longitudinal position midway between quadrupoles, and the holes were round with $\delta_x = \delta_y$. Final emittance was measured 38 lattice periods downstream. A lower lattice strength was used downstream from the mask to allow for the decreased density of the beam. No attempt was made to adjust the transverse velocity distribution to the required distribution for the focusing lattice, so that some mismatch was present. The beamlets thus formed immediately combined. Results for the four cases measured are shown in Table 1. The range of values given for the calculated space charge factor and final emittance is due to the uncertainty in the experimental measurement of the initial emittance. Agreement between theory and experiment is quite good, allowing for the experimental uncertainty. Measurements of the phase space evolution of the combining beams are shown in Fig. 5.

Table 1

a (mm)	δ_x/a	space charge factor	geometric factor	$4\,\epsilon_f$ ($10^{-7}\,\pi$ m-rad) (theory)	(expt)
3.88	1.00	1.16-1.23	1.12	0.78-0.89	0.97
3.88	1.15	1.30-1.41	1.25	0.96-1.07	1.06
3.88	1.30	1.45-1.61	1.39	1.22-1.32	1.19
4.46	1.15	1.36-1.50	1.25	1.17-1.28	1.13

5. Summary

For economic reasons it is desirable to transport the current in a heavy ion inertial fusion linac driver as multiple intense beams at the low energy end of the accelerator, then combine beams as the beam velocity increases. We have described a system which would be used to combine transversely four beams, and have shown theoretically and experimentally that the emittance dilution produced, about a factor of 4, would be within acceptable limits. We find good agreement between simulation, analytical theory, and experiment.

References

[1] F.J. Strückmeier, J. Klabunde, and M. Reiser, Particle Accelerators 15, p. 47 (1974).

[2] I. Hofmann and J. Strückmeier, "3D-Generalized Equations for Emittance and Field Energy of High-Current Beams in Periodic Focusing," GSI Report GSI-86-11, Sept. 1986.

[3] M.G. Tiefenback and D. Keefe, Trans. on Nuc. Sci. NS-32, p. 2483 (1985).

COMPARISON OF ELECTRIC AND MAGNETIC QUADRUPOLE FOCUSING FOR THE LOW ENERGY END OF AN INDUCTION-LINAC-ICF DRIVER*

Charles H. Kim
Lawrence Berkeley Laboratory
University of California
Berkeley, California 94720

Abstract

In this report we compare two physics designs of the low energy end of an induction-linac-ICF driver: one using electric quadrupole focusing of many parallel beams followed by transverse beam combining; the other using magnetic quadrupole focusing of fewer beams without beam combining. Because of larger head-to-tail velocity spread and a consequent rapid current amplification in a magnetic focusing channel, the overall accelerator size of the design using magnetic focusing is comparable to that using electric focusing.

Introduction

The induction linac is an efficient accelerator for high current beams with short pulse durations. Unfortunately, the transportable current for a low energy heavy ion beam in a conventional alternating-gradient focusing channel is severely limited by space-charge forces. For the Inertial-Confinement-Fusion (ICF) application, in which the total number of particles is fixed, the requirement for current amplification can reduce the acceleration rate and makes the linac longer. One way to alleviate this problem and increase the efficiency of the accelerator is to use many parallel beams individually focused in electric quadrupole channels. After a significant acceleration, these multiple beams are combined transversely into a fewer number of beams and injected into magnetic quadrupole focusing channels. A conceptual design using this method was described in the Heavy Ion Fusion Accelerator Research Outline Plan [1], in which 64 beams are combined to 16 beams at an energy of 100 MeV. A schematic diagram of the conceptual design is shown in Fig. 1. In the present study we limit ourselves to the region below 100 MeV.

In order to benefit from the multiple-beam idea, one can use a great number of beams with very small channel diameters [2]. The required mechanical tolerances and beam manipulations associated with bending and combining are not a trivial task. In bending the beams, it is necessary that either a time dependent bending field should be used or the head-to-tail velocity spread has to be removed before bending. Also, recent studies have shown that the transverse emittances tend to grow during the combining operation as the beams see each other's space charge forces [3]. The purpose of the present study is to find what penalties, if any, we need to pay to eliminate the beam combining operation.

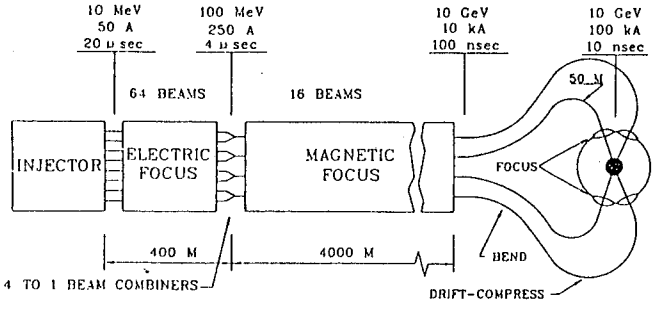

XBL 865-1965A

Fig. 1. A schematic diagram of a conceptual induction-linac-ICF driver using mass number 200 and charge state 3. (Adopted from ref. 1)

*This work was supported by the Office of Energy Research, Office of Basic Energy Sciences, U.S. Department of Energy under Contract No. DE-AC03-76SF00098.

An alternative design presented here uses magnetic quadrupole focusing of fewer beams and does not require beam combining. This simpler option has received less attention so far because the overall size of the accelerator was considered to be too large. However, magnetic focusing channels accept larger head-to-tail velocity spread than electric channels and thus current amplification can take place more rapidly. By taking advantage of these properties, the size of the lower energy end of the driver and the injector can be greatly reduced.

Design Considerations

At injection, the zero-intensity phase advance of the betatron oscillation per lattice period (betatron tune or σ_0) is chosen to be 80 degrees. This value of σ_0 is maintained constant for the head of the beam by increasing the lattice period along the linac. (One can also get the same result by keeping the lattice period constant and increasing the pole-tip field strength provided that the field gradient has not reached the technological limit set by insulator flash-over. Current amplification is faster for this option.). The value of σ_0 for the tail of the bunch decreases as it gets more acceleration than the head of the bunch. The acceleration and bunching schedule is adjusted in such a way that, for the tail of the beam, the tune is allowed to drop as low as 40 degrees but not below this value. This range of values for σ_0 corresponds to a head-to-tail velocity tilt of about 30 per cent for electric focusing channels and 60 per cent for magnetic focusing channels.

Quadrupole occupancy factor is assumed to be 0.5, that is, the physical length of quadrupoles are about one half of the lattice-half period. For higher energy regions beyond 100 MeV, the occupancy factor is decreased to make room for more accelerating units.

The quadrupole-bore radius is kept constant for simplicity. The center-to-center beam separation is also assumed to be constant to avoid beam bending. The pole-tip fields are kept constant along the linac.

Other common design parameters are listed below.

Mass Number	200
Charge State	+3
Injection Energy	10 MeV
Final Energy	100 MeV
Final Current	250 A (Electrical)
Final Pulse Duration	4 micro-seconds
Max Gradient	0.4 MV/m
Max Flux	0.5 Vs/m (Set by size)
Total Charge	1000 micro-Coulombs (electrical)

Description of the Designs

The current amplification schedule is determined by requiring that the maximum beam radius (in the middle of the focusing lenses) remains approximately constant. For the transport channels described in the previous section,

beam current should be amplified linearly with the velocity of the beam for electric focusing and linearly with the kinetic energy for magnetic focusing [4]. For the electric focusing design however, the initial and final currents given in reference 1 require that the current should amplify approximately as velocity to the 1.4-th power. As a result, the beam radius increases along the linac and the quadrupole bore radius is somewhat under-utilized at the injection point. The current amplification schedules adopted in this report are shown in Fig. 2(a) for electric and 3(a) for magnetic focusing.

The total current required at injection is twice higher for electric design (50 A total), but the current per beam at injection is twice higher for magnetic focusing (1.56 A per beam). A design tradeoff can be made for an even smaller injection current with a longitudinal drift compression.

The accelerating voltage waveforms are calculated according to the design procedure described by Kim and Smith [5]. This procedure is based on the current self-replicating scheme where the current pulse shape at a given location is self-similar at subsequent locations. The accelerating voltage waveforms should provide not only the acceleration but also the velocity tilt necessary for current amplification. Two types of voltage waveforms are used; "square" waveforms for accelerations and "triangular or trapezoidal" waveforms for generating the head-to-tail velocity spread for the desired current amplification. Typical waveforms selected at intervals of every 15 meters are shown in Fig. 2(b) for electric and 3(b) for magnetic focusing. Space-charge effects and corrections for the accumulated errors can be added to these waveforms as demonstrated in the LBL multiple beam experiment [6].

At a given location the beam radius may change in time because of the velocity tilt. If the beam current is constant in time, the major radius of the beam cross section (ellipse) remains approximately constant for electric focusing. The same is true for magnetic focusing if the line charge density is constant in time. In the present study, we will consider the constant current distribution for both eletric and magnetic focusing.

The head-to-tail velocity tilt as a function of distance (z) is shown in Figs. 2(c) and 3(c). Velocity spread of up to 30% has been tried in MBE-4 successfully [7]. High velocity tilt in magnetic focusing has not been tried experimentally but calculations using beam envelope equations showed no ill effects. In these calculations, a constant current (at a given location) was assumed for electric focussing and a constant density (at a given location) waa assumed for magnetic focussing [4]. The overall length of the linac depends sensitively on the maximum allowable velocity tilt.

The kinetic energies for the head, center and the tail of the beam bunch are shown in Figs. 2(d) and 3(d) for the two designs. In both designs rapid acceleration happens only after the pulse is significantly compressed.

Other beam parameters are summarized in Table I. The space-charge depressed betatron tune (σ) for magnetic focusing is 15 degrees at the beginning and drops to 7 degrees at the end (for a normalized emittance of $2\times10^{-7}\,\pi$ radian-meters).

The half-lattice period can be increased in steps in combination with some variations of the pole-tip field. Although the required volt-seconds are less for the

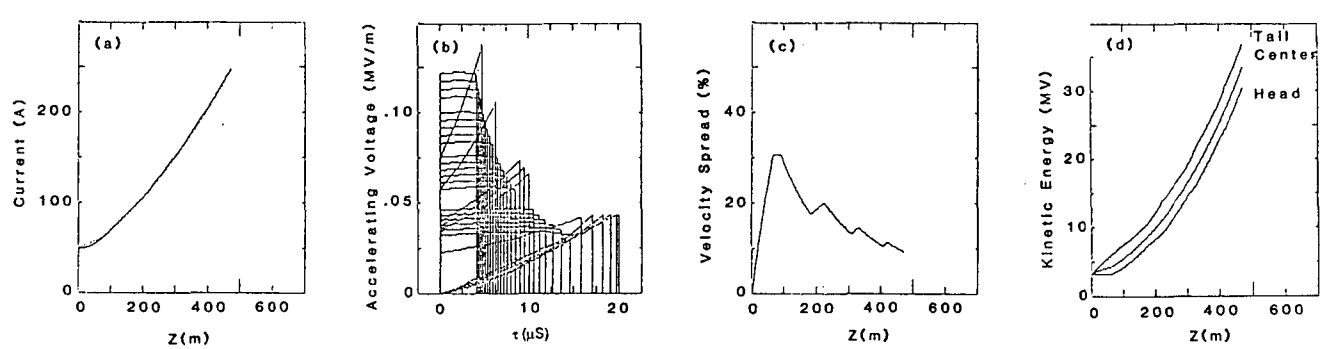

XBL 873-1325

Fig. 2. Design using electrical quadrupole focusing: (a) Current amplification, dotted line shows a schedule which is proportional to $\beta^{1.4}$; (b) Accelerating voltage waveforms selected at every 15 meters; (c) Head-to-tail velocity tilt; (d) Kinetic energies of the head, center, and tail of the beam.

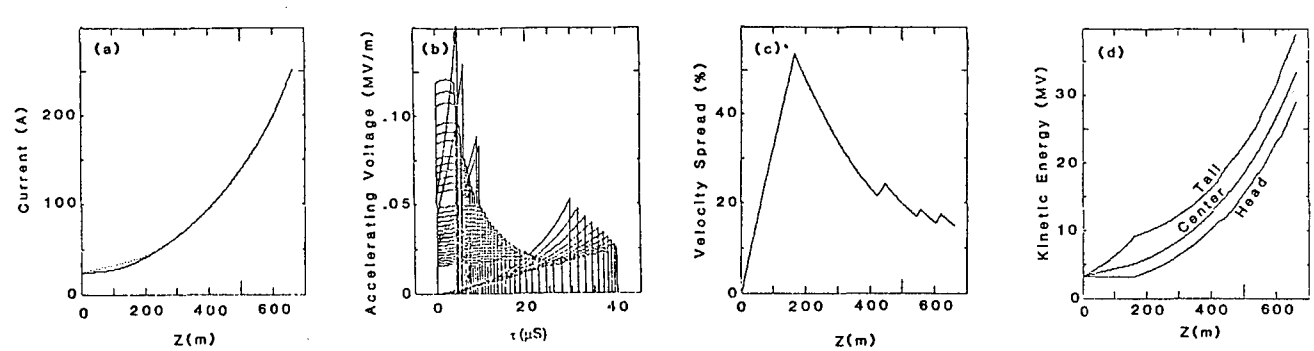

XBL 873-1326

Fig. 3. Design using magnetic quadrupole focusing: (a) Current amplification, dotted line shows a schedule which is proportional to β^2; (b) Accelerating voltage waveforms selected at every 15 meters; (c) Head-to-tail velocity tilt; (d) Kinetic energies of the head, center, and tail of the beam.

Table I. Summary of parameters for the two designs

	Electric	Magnetic
Current at injection	50 Amperes	25 Amperes
Number of beams	64	16
Pulse duration	20 microsec	40 microsec
Beam radius (max)		
Initial	2.7 cm	4 cm
Final	3.4 cm	4 cm
Bore radius	5 cm (constant)	7 cm (constant)
Bunch length		
Initial	62 m	124 m
Final	39 m	39 m
Pole-tip Voltage/field	100 kV (constant)	1.5 T (constant)
Half-lattice period		
Initial	50 cm	50 cm
Final	163 cm	100 cm
Max velocity tilt	30 %	55 %
Total flux required	227 Volt-sec	330 Volt-sec
Total length of Linac	471 meters	660 meters

electrical design the amount of core material is about the same for both designs because the total diameter of the transport structure is bigger for the electrical design.

Beam combining adds some additional length to the electric design. An additional two-bunch lengths of linac is needed if the velocity spread is to be removed before combining and to be restored thereafter.

Possible Improvements

A possible way to improve the electrical design is to increase the injection current by increasing the number of beams and decreasing the individual quadrupole-bore diameter at the same time. However, better alignments are needed [4], the core ID becomes larger, and the combining operation becomes more complex.

A possible way to improve the magnetic design is to use higher pole-tip field. The field at injection can not be increased much because the quadrupoles become too short, but it can be increased linearly with the beam velocity if the half-lattice period is fixed. This scenario allow much faster current amplification (as velocity to the third power) and more rapid acceleration. The tune depression is very strong but may not cause any ill effects if the beam pipe has a round cross section. [8].

Summary

Judging from the size and complexity of the accelerator the design using magnetic focusing appear to be more attractive than that using electric focusing. However, a detailed cost analysis is required to make a final decision. Some of the assumptions made for the magnetic design require further investigation: Magnet-winding techniques for short quadrupoles need to be developed; beam transport with a high velocity tilt need to be experimentally demonstrated.

The author wishes to acknowledge helpful discussions with and suggestions by Drs. T.J. Fessenden, D. Keefe, and L.J. Laslett.

References

[1] LBL Heavy Ion Fusion Staff, "Heavy Ion Fusion Accelerator Research, An Outline Plan", Lawrence Berkeley Laboratory Report, PUB-5178, (1986).

[2] A.Maschke, "MEQALAG: A New Approach to Low Beta Acceleration", Brookhaven National Laboratory Report, BNL-51029 (1979).

[3] C.M.Celata, A.Faltens, D.L.Judd, L.Smith, and M.Tiefenback, "Transverse Combining of Nonrelativistic Beams in a Multiple Beam Induction Linac, in these Proceedings.

[4] C.H.Kim, "High-Current Beam Transport With Multiple Beam Arrays", AIP Conference Proceedings 139, "High Current, High Brightness, and High Duty Factor Ion Injectors", edited by G.H.Gillespie, Y.-Y. Kuo, D. Keefe, and T.P.Wangler, 63 (1985).

[5] C.H.Kim and L.Smith, "A Design Procedure for Acceleration and Bunching in an Ion Induction Linac", Particle Accelerators,vol.18, 101(1985).

[6] T.J.Fessenden, D.Keefe, C.H.Kim, H.Meuth, and W.I.Warwick, "The LBL Multiple Beam Experiments", in these proceedings.

[7] C.H.Kim, D.L.Judd, L.J.Laslett, L.Smith, and A.I.Warwick, "Head-to-Tail Velocity Tilt in an Ion Induction Linac", AIP Conference Proceedings 152, "Heavy Ion Inertial Fusion", edited by M.Reiser, T.Godlove, and R.Bangerter, 264(1986).

[8] I.Haber, "Threshold for Emittance Growth of A-G Focused Intense Beams", ibid., 236(1986).

PUBLICATIONS AND INTERNAL NOTES

HI-FAN-341
LBL-22211
Celata

C.M. Celata, A. Faltens, David L. Judd, L. Smith, M.G. Tiefenback,
"Transverse Comining of Nonrelativistic Beams in a Multiple Beam Induction Linac," Proceedings of the 1987 Particle Accelerator Conference, March 16-19, 1987, Washington, D.C.

HIFAN-342
LBL-22214
Celata

C.M. Celata,
"Transverse Dynamics of Space-Charge-Dominated Ion Beams," Proceedings of the 1987 Particle Accelerator Conference, March 16-19, 1987, Washington, D.C.

HIFAN-344
LBL-22216
Lee

E.P. Lee, E. Close and L. Smith,
"Space Charge Effects in a Bending Magnet System," Proceedings of the 1987 Particle Accelerator Conference, March 16-19, 1987, Washington, D.C.

HIFAN-345
LBL-22217
Fessenden

T.J. Fessenden, D. Keefe, C.H. Kim H. Meuth, and A.I. Warwick,
"The LBL Multiple Beam Experiments," Proceedings of the 1987 Particle Accelerator Conference, March 16-19, 1987, Washington, D.C.

HIFAN-346
LBL-22272
Kim

C.H. Kim,
"Comparison of Electric and Magnetic Quadrupole Focusing for the Low Energy End of an Induction-Linac-ICF Driver," Proceedings of the 1987 Particle Accelerator Conference, March 16-19, 1987, Washington, D.C.

HIFAN-347
LBL-22274
Gough

D. Gough, D. Brodzik, A. Faltens, C. Pike, and J. Stoker,
"Pulsers for the Induction Linac MBE-4," Proceedings of the 1987 Particle Accelerator Conference, March 16-19, 1987, Washington, D.C.

HIFAN-348
LBL-22275
Tiefenback

M.G. Tiefenback,
"Emittance Growth in Mismatched Space-Charge-Dominated Beams," Proceedings of the 1987 Particle Accelerator Conference, March 16-19, 1987, Washington, D.C.

HIFAN-349
LBL-22411
Keefe

D. Keefe,
"Prospects for Fusion Power," to be published in the Journal of Fusion Energy.

HIFAN-350
LBL-22349
HIF Staff

HIF Staff,
"Year End Report, April 1, 1986 - September 30, 1986"

HI-FAN-351
LBL-22421
Lee

E. P. Lee, J. Hovingh, A. Faltens, and D. Keefe,
"Heavy Ion Fusion System Assessment Project, Quarterly Status Report, January-March, 1986," Lawrence Berkeley Laboratory (10/86).

HI-FAN-352
LBL-22465
Tiefenback

Michael G. Tiefenback,
"Space-Charge Limits on the Transport of Ion Beams in a Long Alternating Gradient System," Ph.D. Thesis, University of California, Berkeley (8/86).

HIFAN-353
Kim

C.J. Kim and S. McCreight,
"Pulse Shaping of a Nonrelativistic Heavy Ion Beam" (11/11/86).

HI-FAN-354
LBL-22713
Hovingh

J. Hovingh, V. O. Brady, A. Faltens, D. Keefe, and E. P. Lee,
"Analysis of an Induction Linac Driver System for Inertial Fusion," (12/86).

HI-FAN-355
LBL-22714
Hovingh

J. Hovingh, V. O. Brady, A. Faltens, D. Keefe, and E. P. Lee,
"Heavy Ion Linear Induction Accelerators as Drivers for Inertial Fusion Power Plants," December, 1986.

HI-FAN-356
LBL-22757
Hovingh

J. Hovingh, V. O. Brady, A. Faltens, D. Keefe, and E. P. Lee, "Heavy Ion Linear Induction Accelerators as Drivers for Inertial Fusion Power Plants," December, 1986; to be published in Fusion Technologies; (12/86).

HIFAN-357
Nelson

D. Nelson and D.A. Van Dyke,
"Summary of Measurements and Sorting of Neodymium-Iron-Boron (Rare Earth) Magnet Array (Group A Sumitoto Neomax - 30H) & (Group B Vacuumschmelze Vacodym - 370)" (2/5/87)

HIFAN-358
Laslett

Jackson Laslett,
"Eddy Currents Induced in a Thin-Walled Circular Conducting Cylinder by an Externally Applied Quadrupole Field" (2/5/87)

HIFAN-359
LBL-22990
Kalnins

J.G. Kalnins, L. Smith,
"Emittance Growth Due to Mismatch in a Constant Focussing Channel," February 1987.

HIFAN-360
LBL-23040
Lee

E.P. Lee, A. Faltens, and D. Keefe,
"Heavy Ion Fusion System Assessment: Final Focus and Transport Model," February 1987.

HIFAN-361
Heckman

H.H. Heckman, H.R. Bowman, Y.J. Karant, J.O. Rasmussen, A.I. Warwick, and Z.Z. Xu
"Range-Energy Relation for Au Ions, E/A 150 MeV" (3/3/87)

HIFAR NOTES (Internal and Informal)

HIFAR Note-104 Brodzik	D. Brodzik, "ITT Tubes" (10/6/86)
HIFAR Note-105 Herrmannsfeldt	W.B. Herrmannsfeldt, "C^+ Guns for Ilse (About 1 Amp)"
HIFAR Note-106 Keefe	D. Keefe, "Energy Analysis for MBE-4," (10/13/86)
HIFAR Note-107 Laslett	L.J. Laslett, "Illustrations of Some Scaling Laws for Transverse Focusing by Electrostatic Quacrupole Lenses" (10/10/86)
HIFAR Note-108 Judd	D.L. Judd, On Double Bends for Beam Merging," July 1986
HIFAR Note-109 Hovingh	J. Hovingh "Number of Half Period Lengths in a Reference Accelerator," October, 1986.
HIFAR Note-110 Smith	L. Smith, "MBE-4 g-Factor Revisited," October, 1986.
HIFAR Note-111 Hovingh	J. Hovingh, "Effect of Changes of Beamlet Clearance and Pulse Rise Time in LIACEP On Accelerator Cost and Performance," October, 1986.
HIFAR Note-112 Fessenden	T. Fessenden, "Why ILSE? What ILSE?," December, 1986.
HIFAR Note-113 Lee	E. Lee, Letter to T. Godlove with Enclosure by J. Hovingh on LIACEP Cost Escalation, December, 1986.
HIFAR Note-114 Faltens	A. Faltens, "High-Voltage, High Gradient Heavy Ion Injectors" (12/5/86)

HIFAR Note-115
Judd
D. Judd,
"Approximate K-V Periodic-Envelope Parameters of Symmetric FODO Transport Lattices for Intense Beams" (12/86)

HIFAR Note-116
Judd
D. Judd,
"Various Magnetic Uniform-Field Regions Produced by Current-Sheet Pairs" (12/86)

HIFAR Note-117
Judd
D. Judd,
"Simple General Derivation of the Familiar Approximate Relation for Head-To-Tail Velocity Tilt" (12/86)

HIFAR Note-118
Judd
D. Judd and J. Laslett,
"List of Uncertainties About ILSE" (12/86)

HIFAR Note-119
Lee
E. Lee,
"ILSE/First Try Conceptual Design" (12/16/86)

HIFAR NOTE-120
Laslett
J. Laslett
"ILSE Reference Case Beam Transport After Merging" (12/17/86)

HIFAR Note-121
Hovingh
Jack Hovingh,
"Velocity Tilt Limits for LIACEP," (12/86).

HIFAR Note-122
Hovingh
J. Hovingh,
"LIACEP Versions" (12/19/86)

HIFAR Note-123
Judd
D.L. Judd,
"Combining Beams in ILSE - Notes for Orientation," Prepared 12/18/86, Presented January 8, 1987

HIFAR Note-124
Faltens
A. Faltens,
Vugraphs from Talk on: Pulsed Quadrupoles (1/15/87)

HIFAR Note-125
Laslett
J. Laslett,
Some Comments Pertaining to ILSE As of January 12, 1987 Especially now Pertaining to Pulsed Ferromagnetic Quadrupoles, of a Type Discussed with A. Faltens for use at 4 MeV Following Merging. (1/20/87)

HIFAR Note-126
Laslett

J. Laslett,
"Relations Concerning the Phase Plot of Maximum-Amplitude Individual Particle at a Given Location" (1/20/87)

HIFAR Note-127
Laslett

J. Laslett,
"On Matching A Merged Beam" 2/5/87

HIFAR Note-128
Faltens

A. Faltens,
Miscellaneous Contributions to ILSE (2/18/87)

HIFAR Note-129
Laslett

L. Jackson Laslett,
"Some Examples and Implications of Velocity Tilts for the Ilse Design" (2/18/87)

HIFAR Note-130
Lee

E. Lee, T. Fessenden, C. Celata, and L. Smith,
"LBL HIF Presentation to LLNL X Division" (2/19/87

HIFAR Note-131
Laslett

J. Laslett,
"The Possibility of Magnetic Transport Following A Merge at 2.0 MeV" (2/21/87)

HIFAR 132
Faltens

Andris Faltens,
"On Merging of a Beam with Energy Tilt," March 1987.

HIFAR Note-133
Brady

V. Brady,
"Pulsed Iron-Dominated Quadrupoles for ILSE," March 3, 1987.

HIAR NOTE-134
Laslett

Jackson Laslett,
"Intense Merged Beams of C^{+1} At 2.0 MeV.," March 11, 1987.

HIFAR NOTE-135
Laslett

Jackson Laslett
"Some Focusing Options for ILSE" March 11, 1987.

HIFAR NOTE-136
Brodzik

D. Brodzik,
"Sec. D. Waveforms," HIFAR Note-136, March 17, 1987.

H.I.F. STAFF ROSTER

Denis Keefe

Donald A. Brodzik
Warren Chupp
Robert D. Edwards
Andris Faltens
Thomas J. Fessenden
William B. Ghiorso
David Gough
Wayne Greenway
Ralph Hipple
Cai Houston
Charles H. Kim
Bruce MacDonell
John Meneghetti
Hermann Meuth
Harry Meyer
Joseph Perez
Chester D. Pike
Thomas Purtell
James Rice, Jr.
Henry L. Rutkowski
Stuart Ryce
Gerald L. Stoker
Bill Tiffany
Mike Towler
David Vanecek
Gerald W. West

Lloyd Smith

Victor Brady
Christine Celata
Elon Close
David L. Judd
L. Jackson Laslett
Edward P. Lee

William B. Herrmannsfeldt, SLAC

Jack Hovingh, LLNL

HALF-YEAR/YEAR-END REPORT: DISTRIBUTION LIST

Allied Chemical Corporation

Carl Smith

Argonne National Lab.

Thomas A. Fields
Ronald Martin

University of Arizona

R. Morse

Batelle

John Hartman

Bechtel

W. Allen

BMD/ATC/SDC

Milton Hawie
Brian Strickland

Brookhaven National Lab.

Mark Barton
E. Courant

C.E.A. Bruyeres-le-Chatel

R. Dei-Cas

CEBAF

J. Bisognano
D. Douglas
H. Grunder
G. Krafft
C. Leemann

University of Calif., Irvine

Norman Rostoker

Cornell University

John Nation
Ravi N. Sudan

DARPA

H. Lee Buchanan

Department of Defense (SDIO)

Richard Gullickson
W. Higgins

Department of Energy

DP-OIF

Gregory D'Alessio
Sheldon L. Kahalas
R. Schriever
Marshall Sluyter

ER

Ryszard Gajewski (AEP)
Gerry Peters (HENP)
W. Polansky (AEP)
Robert Rader (OPA)
D. Stevens (BES)
David F. Sutter (HENP)
Alvin Trivelpiece, Dir.,
Office of Energy Research
William Wallenmeyer (HENP)

DoE San Office

Rudolf Bredderman
Dennis Neely

E.P.R.I.

Robert Scott

Fermi National Accelerator Lab.

Frank T. Cole
Fred Mills
Lee Teng

F.O.M. Amsterdam

F. Siebenlist

GANIL

P. Lapostolle

GE

John Lucek

GSI

R. Bock
D. Boehne
I. Hofmann
A. Warwick

University of Illinois

G. Miley

Institute for Nuclear Study

Y. Hirao

KMS Fusion, Inc.

Alex Glass

Kanazawa University

S. Kawasaki

Lawrence Berkeley Laboratory

D. Atwood, 80/101
R. Avery, 46/189
K. Berkner, 50/149
D. Brodzik, 46/125
C. Celata, 47/112
W.W. Chupp, 47/112
M. Cornacchia, 47/112
T. Elioff, 90/4040
A. Faltens, 47/112
T. Fessenden, 47/112
A. Garren, 47/112
D. Gough, 47/112
E. Hartwig, 47/112
H. Heckman, 50/245
T. Henderson, 46/161
E. Hoyer, 46/187
E. Hyde, 50A/4133E
R. Johnson, 50A/4119
D. Judd, 47/112
D. Keefe, 47/112
C. Kim, 47/112
M. Krebs, 50A/4112
W. Kunkel, 4/230
G. Lambertson, 47/112
L.J. Laslett, 47/112
E.P. Lee, 47/112
E. Lofgren, 47/112
J. Marx, 50/149
J. Meneghetti, 46/161
H. Meuth, 47/112
J. Peterson, 90/4040
C. Pike, 47/112
H. Rutkowski, 47/112
A. Sessler, 4/230
D. Shirley, 50A/4133
L. Smith, 47/112
C. Taylor, 46/161
D. Vanecek, 58/1011
D. Vaughan, 50/149

Lawrence Livermore Laboratory

Roger Bangerter, L-477
W. Barletta, L-626
Richard J. Briggs, L-321
John L. Emmett, L-488
Dennis Hewitt, L-472
Darwin Ho, L-477
John Holzrichter, L-481
William Kruer, L-472
William Krupke, L-488

Lawrence Livermore Laboratory (cont'd)

Bruce Langdon, L-472
J. Lindl, L-477
Jim Mark, L-477
John Nuckolls, L-477
Louis Reginato, L-526
Erik Storm, L-481

Lockheed

John Siambis

Los Alamos National Laboratory

Ihor Bohachevsky
Richard Cooper
Robert Jameson
Tom MacDonald
Earl Meyer
Roger B. Perkins
Richard Stokes
Tai-Sen Wang
Doug Wilson

University of Maryland

Martin Reiser
Derek Tidman

Max Planck Inst. fur Plasma Physik Garching

Arnulf Schluter

Maxwell Laboratories

Library

National Bureau of Standards

S. Penner
M. Wilson

Naval Research Lab.

Steven Bodner
T. Coffey
Terry Godlove
Irving Haber
Philip Sprangle
Peter Turchi

Occidental Research Corp.

Wyn Salisbury

Osaka University

T. Mochizuki
C. Yamanaka

Universita di Padova

A. Pascolini
M. Pusterla

Physical Dynamics

G. H. Gillespie

Physics International

Library

Pulse Sciences, Inc.

Ian Smith
Kurt Nielson
M. Tiefenback

RAFAEL

Joseph Shiloh

Rutherford Laboratory

John D. Lawson
Chris Pryor
Graham Rees

Sandia Laboratories

Everet H. Beckner
Don Cook
Glenn Kuswa
Tom Martin
J.P. VanDevender

W.J. Schafer Associates

Michael J. Monsler

SLAC

William Herrmannsfeldt, Bin 26
Burton Richter, Bin 7

Soka University

Tetsuya Saito

SOREQ Nuclear Research Center

A. Sternlieb

TITAN Systems, Inc.

Ken Billman
G. Yonas

TRW

J. Gordon
Z. Guiragossian
J. Maniscalco
A.W. Maschke
W. Steele

UCLA

John Dawson

University of Texas at Austin

Toshi Tajima

URA

Edward Knapp

Varian

S.S. Rosenblum

Westinghouse

M. Nahemow
E. W. Sucov

University of Wisconsin

G. Kulcinski
G. Moses
R. Peterson

This report was done with support from the Department of Energy. Any conclusions or opinions expressed in this report represent solely those of the author(s) and not necessarily those of The Regents of the University of California, the Lawrence Berkeley Laboratory or the Department of Energy.

Reference to a company or product name does not imply approval or recommendation of the product by the University of California or the U.S. Department of Energy to the exclusion of others that may be suitable.

LAWRENCE BERKELEY LABORATORY
TECHNICAL INFORMATION DEPARTMENT
UNIVERSITY OF CALIFORNIA
BERKELEY, CALIFORNIA 94720